AN EXPANDING MANIFOLD CHARACTERIZES ADOLESCENT RECONFIGURATIONS OF STRUCTURAL CONNECTOME ORGANIZATION

Bo-yong Park[a*], Richard A. I. Bethlehem[b,c], Casey Paquola[a], Sara Larivière[a], Raul R. Cruces[a], Reinder Vos de Wael[a], Neuroscience in Psychiatry Network (NSPN) Consortium[1], Edward T. Bullmore[c], Boris C. Bernhardt[a*]

[a]McConnell Brain Imaging Centre, Montreal Neurological Institute and Hospital, McGill University, Montreal, Quebec, Canada; [b]Autism Research Centre, Department of Psychiatry, University of Cambridge, Cambridge, United Kingdom; [c]Brain Mapping Unit, Department of Psychiatry, University of Cambridge, Cambridge, United Kingdom;

***Corresponding Authors:**

Boris C. Bernhardt, PhD
Multimodal Imaging and Connectome Analysis Lab
McConnell Brain Imaging Centre
Montreal Neurological Institute and Hospital
McGill University
Montreal, Quebec, Canada
Phone: +1-514-398-3579
Email: boris.bernhardt@mcgill.ca

Bo-yong Park, PhD
Multimodal Imaging and Connectome Analysis Lab
McConnell Brain Imaging Centre
Montreal Neurological Institute and Hospital
McGill University
Montreal, Quebec, Canada
Email: bo.y.park@mcgill.ca

[1]A complete list of investigators from the Neuroscience in Psychiatry Network (NSPN) Consortium can be found in the Supporting Information.

ABSTRACT

Adolescence is a critical time for the continued maturation of brain networks. Here, we assessed structural connectome development in a large longitudinal sample ranging from late child- to young adulthood. Using novel techniques that project high-dimensional connectomes into compact manifold spaces, we could identify a marked expansion of structural connectomes with the strongest effects in transmodal regions during adolescence. Findings were reflected increased within-module connectivity together with increased segregation, indicating an increasing differentiation of higher order association networks from the rest of the brain. Projection of subcortico-cortical connectivity patterns into these manifolds showed parallel alterations in pathways centered on the caudate and thalamus. Connectome findings were contextualized via spatial transcriptome association analysis, highlighting genes enriched in cortex, thalamus, and striatum. Finally, we could show with statistical learning that cortico-subcortical manifold features at baseline and their maturational change predicted measures of intelligence at follow-up, supporting utility of connectome manifolds to bridge structural network reconfigurations and cognitive outcomes in adolescent development.

KEYWORDS: neurodevelopment; adolescence; connectome manifold; longitudinal; MRI; cognition; multi-scale

INTRODUCTION

Adolescence is a time of profound and genetically mediated changes in whole-brain network organization (Larsen and Luna, 2018; Menon, 2013). Adolescent development is important for overall maturation in cognitive and educational functions and brain health more generally, a notion reinforced by the overlapping onset of several neurodevelopmental and psychiatric disorders (Hong et al., 2019; Khundrakpam et al., 2017). With increased capacity to carry out longitudinal studies in large samples, it is now possible to track changes in brain network organization within subjects, providing mechanistic insights into maturational processes, their biological underpinnings, and their effects on behavior and cognition.

By offering an *in vivo* window into brain organization, neuroimaging techniques such as magnetic resonance imaging (MRI) offer the ability to track adolescent development over time, and to explore associations to cognitive functions. Early cross-sectional and longitudinal studies focused on the analysis of morphological changes (Gogtay et al., 2004; Shaw et al., 2006; Tamnes et al., 2017), including cortical thickness (Shaw et al., 2006; Tamnes et al., 2017) and volume measures (Gogtay et al., 2004; Tamnes et al., 2017), with initial grey matter increases until late childhood followed by a decline for the rest of the lifespan. More recent work explored changes in intracortical microstructure, capitalizing on myelin-sensitive contrasts such as magnetization transfer ratio (MT) mapping, which generally suggest overall increases in adolescence (Paquola et al., 2019a; Whitaker et al., 2016) together with depth dependent shifts in intracortical myelin profiles (Paquola et al., 2019a). Besides the increasingly recognized changes in cortico-cortical connectivity, additionally studying subcortical regions offer additional insights for understanding brain maturation during adolescence. Indeed, an increasing body of connectome level studies emphasizes that subcortical structures contribute significantly to patterns of whole-brain organization, dynamics, and cognition (Hwang et al., 2017; Müller et al., 2020; Shine et al., 2019). In prior neurodevelopmental studies, it has been shown that the volumes of the striatum and thalamus decrease between adolescence and adulthood, potentially paralleling processes resulting in cortical grey matter reduction during this time window (Herting et al., 2018). A close inter-relationship between cortical and subcortical development is also suggested by recent functional connectivity work suggesting that cortico-subcortical pathways are intrinsically remodeled during adolescence (Váša et al., 2020), and these changes affect cognitive functioning. Collectively, these prior findings suggest measurable trajectories of cortical and subcortical structural organization and support associations to cognitive development (Baum et al., 2020; Shaw et al., 2006).

Recent conceptual and methodological advances have increasingly emphasized the analysis of brain networks as being the way forward to study brain organization, development, and substrates underlying cognitive trajectories in humans. One key modality to track developmental changes in structural connectivity is diffusion MRI (dMRI), a technique sensitive to the displacement of water in tissue that allows for the non-invasive approximation of inter-regional white matter tracts. Prior cross-sectional and longitudinal studies in children and adolescents outlined changes in the microstructure of major white matter tracts during development based on the analysis of dMRI derived tissue parameters (Lebel and Beaulieu, 2011; Schmithorst and Yuan, 2010). These findings have been complemented by assessments of brain network topology using graph-theoretical analysis (Oldham and Fornito, 2019), which reported a relatively preserved spatial layout of structural hubs across adolescent development on the one hand (Hagmann et al., 2010), yet with a continued strengthening of their connectivity profiles, likely underpinned by the ongoing maturation of long-range association fibers (Lebel and Beaulieu, 2011; Oldham and Fornito, 2019). One emerging approach to synoptically address connectome organization and development comes from the application of manifold learning techniques to connectivity datasets. By decomposing whole-brain structural and functional connectomes into a series of lower dimensional axes capturing spatial gradients of connectivity variations (Margulies et al., 2016; Vos de Wael et al., 2020), these techniques allow for the analysis of local connectivity changes within the context of macroscale motifs of brain

wiring. Gradients derived from a variety of techniques have been shown to be genetically determined and relatively conserved across primate evolution (Valk et al., 2020). Furthermore, functional connectome findings suggest their promise to serve as spatial axes aligned with the cortical hierarchy (Margulies et al., 2016; Mesulam, 1998) and to capture functional activation patterns across different task states (Karapanagiotidis et al., 2020; Mckeown et al., 2020). A recent study furthermore demonstrated that the application of manifold learning techniques to whole-brain dMRI connectomes is feasible, and that these gradients provide a coordinate system to interrogate the coupling between brain structure and functional dynamics (Park et al., 2021). Still, the application of manifold techniques to dMRI connectomes in children and adolescents to track their longitudinal maturations has not been performed. In a recent assessment by our team, manifold learning techniques have been applied to myelin sensitive intracortical MT data, showing an increasing myeloarchitectural differentiation of association cortex throughout adolescence (Paquola et al., 2019a).

Here, we charted developmental changes in structural connectome organization, based on an accelerated longitudinal neuroimaging study from late childhood to early adulthood, covering the entire adolescent time period involving a total of 208 participants investigated between 14 to 26 years of age (Kiddle et al., 2018; Whitaker et al., 2016). Compared to cross-sectional designs, longitudinal studies track within-subject change, separating developmental effects from between-subject variability (Louis et al., 1986). We first estimated longitudinal changes in structural connectome manifolds across age. The compact and lower dimensional space furthermore allowed for the integration of connectome level findings with changes in MRI-based measures of cortical morphology and intracortical myelin. We furthermore projected subcortico-cortical connectivity patterns into the manifold space, to assessed parallel developmental shifts of these pathways in the studied time window. Connectome-manifold changes were contextualized at the molecular level via transcriptomic association and developmental enrichment analyses based on *post-mortem* datasets, which furthermore allowed for data-driven exploration of time windows of spatially co-localized gene sets. To also assess behavioral associations of connectome manifold changes, we harnessed supervised machine learning to predict future measures of cognitive function. Multiple sensitivity analyses were conducted at several steps to verify the robustness of our findings, and analytical code is made fully accessible to allow for independent replication of our findings.

RESULTS

These findings were based on the Neuroscience in Psychiatry Network (NSPN) 2400 cohort (Kiddle et al., 2018; Whitaker et al., 2016). In brief, we studied 208 healthy individuals enrolled in an accelerated longitudinal study, where several age-stratified cohorts were enrolled to span the time period from adolescence and young adulthood. Participants (48% female) had a mean age of 18.82 years (range = 14–25 years) at baseline and 19.95 years (15–26 years) at follow-up. The average interval between baseline and follow-up scan was 11.28 months (range = 6–12 months). See the *Methods* for details on participant selection, image processing, and analysis.

Macroscale structural connectome manifold

For every participant, we built cortex-wide structural connectome manifolds formed by the eigenvectors displaying spatial gradients in structural connectome organization using non-linear dimensionality reduction techniques (https://github.com/MICA-MNI/BrainSpace) (Vos de Wael et al., 2020). Individual manifolds were aligned to a template manifold estimated from a hold-out dataset (see *Methods*) (Langs et al., 2015; Vos de Wael et al., 2020). Three eigenvectors (E1, E2, and E3) explained approximately 50% of variance in the template affinity matrix, with each eigenvector showing a different axis of spatial variation across the cortical mantle (**Fig. 1A**). Eigenvectors

depicted a continuous differentiation between medial and lateral cortices (E1), between inferior and superior cortices (E2), and between anterior and posterior areas (E3). For each participant and time point, we calculated *manifold eccentricity*, which depicts how far each node is located from the center of the template manifold (see *Methods*). It thus simply quantifies the changes in eigenvectors between the time points in terms of expansion and contraction instead of comparing multi-dimensional connectome manifolds (Bethlehem et al., 2020). The manifold eccentricity showed high values in frontal and somatomotor regions, while temporoparietal, visual, and limbic regions showed low values (**Fig. 1B**).

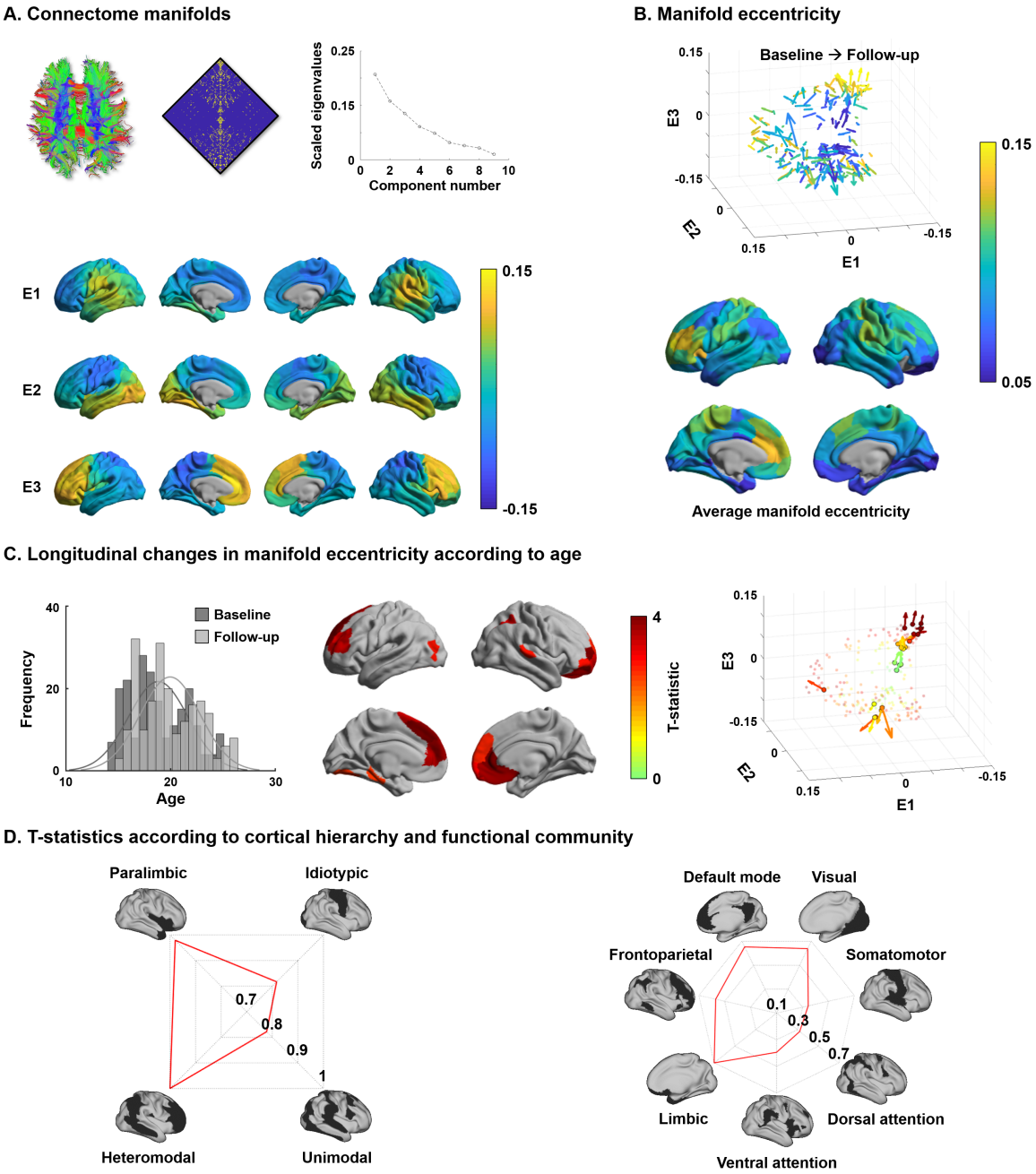

Fig. 1 | Structural connectome manifolds. (A) Systematic fiber tracking based on dMRI generated a cortex-wide structural connectome, which was subjected to diffusion map embedding. As shown in the scree plot, three eigenvectors (E1, E2, E3) explained approximately 50% connectome variance, and each depicted a different gradual transition across the cortical mantle. **(B)** Manifold eccentricity measured by Euclidean distance between the template center and each data point. Arrows depict average positional change in connectivity space from baseline to follow-up. The color of each arrow represents each brain region mapped on the surface on the bottom. **(C)** The histogram represents age distribution of all subjects at baseline and follow-up. The colors on brain surfaces indicate t-statistics of regions showing significant

longitudinal changes in manifold eccentricity across age, following multiple comparisons correction with a false discovery rate (FDR) procedure. Datapoint colors in the scatter plot represent t-statistics. Identified regions are represented with arrows that originate from baseline to follow-up. **(D)** Stratification of age-related changes in manifold eccentricity along cortical hierarchy (Mesulam, 1998) and functional community (Yeo et al., 2011).

Changes in manifold eccentricity across age

Leveraging linear mixed effect models that additionally controlled for effects of sex, site, head motion, and subject-specific random intercepts (Worsley et al., 2009), we assessed changes in manifold eccentricity across age (see *Methods*). Manifold eccentricity expanded as age increased, especially in bilateral prefrontal and temporal areas, as well as left early visual and right lateral parietal cortices (false discovery rate (FDR) < 0.05 (Benjamini and Hochberg, 1995); **Fig. 1C**). Stratifying these effects along four cortical hierarchical levels, defined using an established taxonomy based on patterns of laminar differentiation and tract-tracing data in non-human primates (Mesulam, 1998), we identified peak effects in heteromodal association and paralimbic areas (**Fig. 1D**). Convergent findings were observed when analyzing the effects with respect to intrinsic functional communities (Yeo et al., 2011), showing highest effects in default mode and limbic areas followed by visual and frontoparietal cortices. No significant contraction of manifold eccentricity was observed. In addition, we could not find any significant effects when we fitted the model with a quadratic form of age (*i.e.,* age^2), indicating the manifold eccentricity linearly increases across age.

To conceptualize the findings derived from manifold eccentricity with respect to conventional network topologies, we correlated manifold eccentricity changes with several graph-theoretical measures of structural connectome (**Fig. S1**) (Rubinov and Sporns, 2010). We first defined six spatially contiguous clusters within the regions that showed significant age-related changes in manifold eccentricity (see *Fig. 1C*) and correlated within-subject changes in manifold eccentricity with those in degree centrality, connectivity distance, and modular parameters (*i.e.,* within-module degree and participation coefficient based on modules defined via Louvain's community detection algorithm (Blondel et al., 2008); see *Methods*; **Fig. S2**). We found significant positive associations for degree centrality and within-module degree, suggesting that connectome manifold expansion reflects a concurrent increase of overall connectivity, particularly within modules. Stratifying changes in manifold eccentricity as well as connectome topology measures according to the discretized age bins confirmed these age-related trends (**Fig. S3**). Indeed, except for participation coefficient, values in general increased from childhood to young adulthood.

Effects of cortical morphology and microstructure

Previous studies demonstrated significant changes in cortical morphology and microstructure during adolescence, showing co-occurring reductions in cortical thickness and MT skewness, the latter being an index of depth dependent intracortical myelin changes in multiple lobes (Gogtay et al., 2004; Khundrakpam et al., 2017; Paquola et al., 2019a; Shaw et al., 2006). We replicated these findings by showing cortical thinning in almost all brain regions across the studied age window as well as reductions in depth dependent MT skewness, suggestive of supragranular enrichment of myelin (**Fig. 2A**). To evaluate whether the age-related changes in manifold eccentricity were robust above and beyond these regional changes in cortical thickness and MT, we implemented linear mixed effect models after correcting for cortical thickness and MT from the manifold eccentricity (**Fig. 2B**). While we observed virtually identical spatial patterns of manifold eccentricity changes in models that controlled for thickness, MT skewness, and both, effects in clusters of manifold eccentricity findings were reduced in models that additionally controlled for these values (average reduction of t-value in models controlling for thickness/MT skewness/both = 42/18/68%).

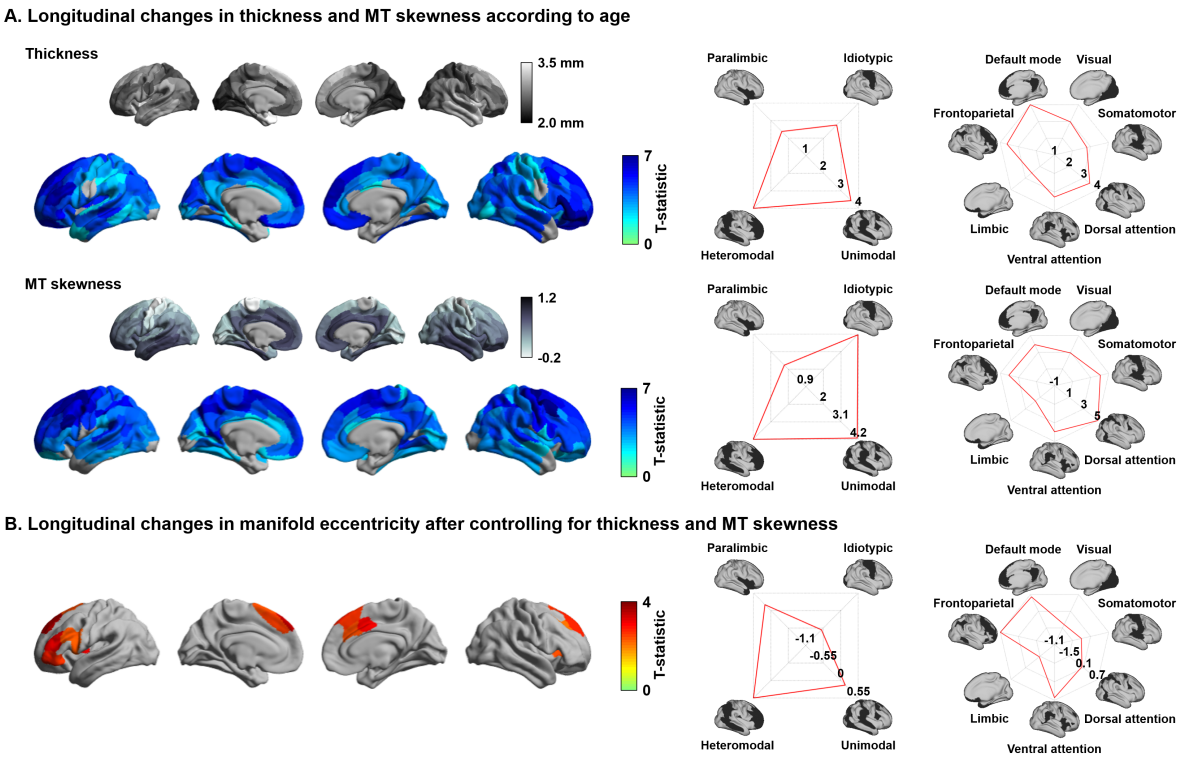

Fig. 2 | Association to morphological and microstructural effects. (A) The t-statistics of identified regions that showed significant age-related changes in cortical thickness (upper row) and MT (bottom row), and stratification of t-statistics according to cortical hierarchy (Mesulam, 1998) and functional community (Yeo et al., 2011). **(B)** Age-related changes in manifold eccentricity after controlling for cortical thickness and MT.

Age-related changes in subcortico-cortical connectivity

Besides visualizing these changes in cortico-cortical connectivity, we also capitalized on the manifold representation to assess adolescent changes in the connectivity of subcortical regions, to obtain a more holistic insight into whole-brain connectome reconfigurations during this time period, and to examine whether subcortical connectivity patterns undergo parallel developmental trajectories (Hwang et al., 2017; Shine et al., 2019). Specifically, we assessed changes in subcortical-weighted manifolds across age, defined by projecting the streamline strength of subcortical regions to cortical targets to the manifold space (see *Methods*). Such an analysis situates changes in subcortico-cortical pathways in the macroscale context of cortico-cortical connectivity identified in the previous analyses. After multiple comparison correction, the caudate and thalamus showed significant effects of subcortical-weighted manifolds (FDR < 0.05; **Fig. 3**), and marginal effects were observed in the putamen, pallidum, and hippocampus (FDR < 0.1).

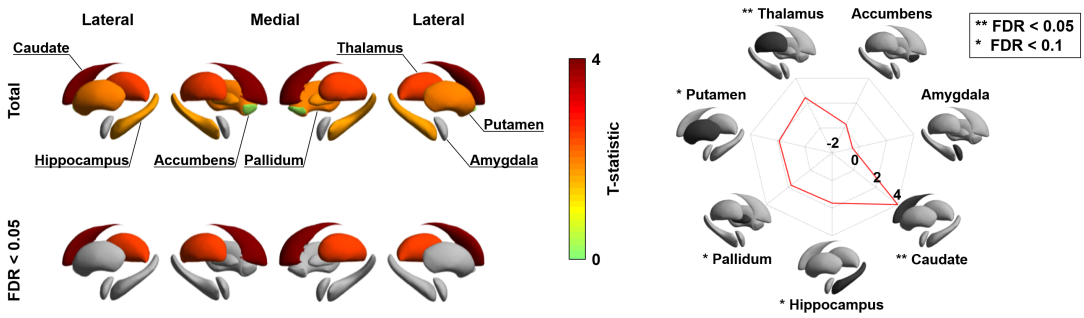

Fig. 3 | Longitudinal changes in subcortical-weighted manifolds. The t-statistics of age-related changes in subcortical-weighted manifolds. The effects of each subcortical region are reported on the radar plot. *Abbreviation:* FDR, false discovery rate.

Transcriptomic association analysis

Connectome organization more generally, and macroscale gradients more specifically, have been argued to reflect genetic expression profiles, underscoring the close link between the physical layout of the brain and innate molecular factors (Buckner and Krienen, 2013; Fornito et al., 2019). Here, we carried out a transcriptomic association and developmental enrichment analyses to contextualize the age-related manifold eccentricity changes with respect to patterns of *post-mortem* gene expression from a sample of independent adults (**Fig. 4A**). Specifically, leveraging mixed effect models, we associated the spatial patterns of manifold change across age that controlled for cortical thickness and MT in the NSPN sample with cortical maps of *post-mortem* gene expression data from the Allen Institute for Brain Sciences (Arnatkeviciute et al., 2019; Gorgolewski et al., 2015, 2014; Hawrylycz et al., 2012; Markello et al., 2020). Among the list of most strongly associated genes (FDR < 0.05), we selected only genes that were consistently expressed across different donors (r > 0.5) (Arnatkeviciute et al., 2019) (**Data S1**). We fed those into a developmental gene enrichment analysis, which highlights developmental time windows across macroscopic brain regions in which genes are strongly expressed (see *Methods*) (Dougherty et al., 2010). This analysis highlighted marked associations between the spatial pattern of longitudinal change in connectome manifold eccentricity and the expression of genes that were found enriched from childhood onwards in the cortex, thalamus, and cerebellum (FDR < 0.001; **Fig. 4B**). Although signal was reduced, genes were also showing an enrichment for expression in the striatum at the transition from childhood to adolescence (FDR < 0.05). On the other hand, identified genes were not found to be expressed in the hippocampus and amygdala.

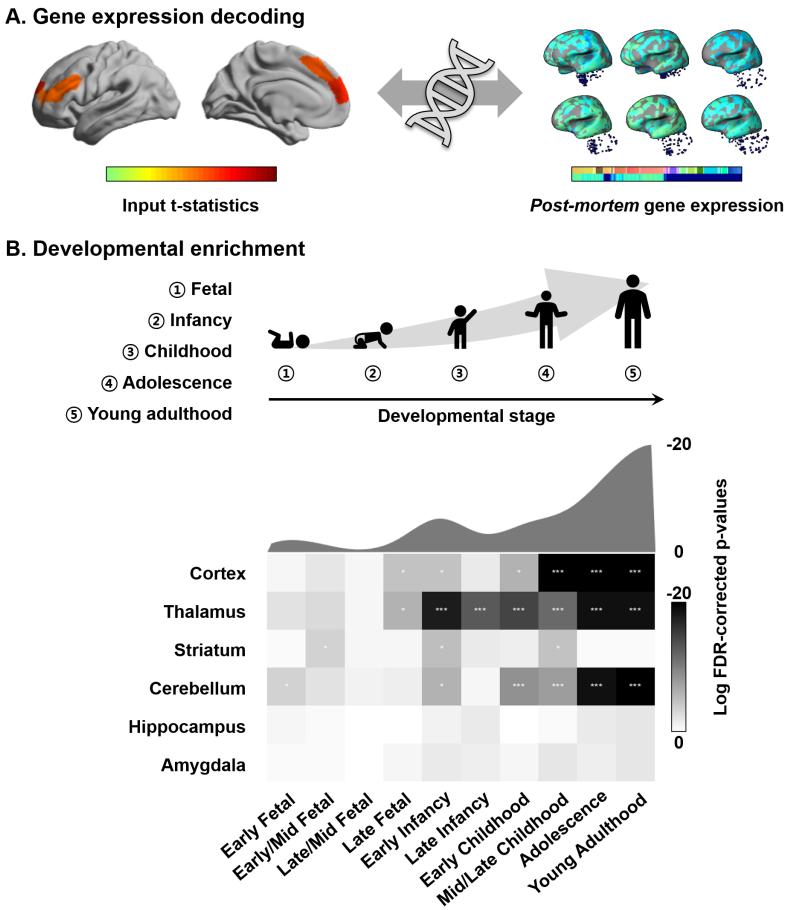

Fig. 4 | Transcriptomic analysis. (A) Gene decoding process by associating t-statistics from the linear mixed effect model with *post-mortem* gene expression maps. **(B)** We identified genes that were spatially correlated with the input t-statistic map (false discovery rate (FDR) < 0.05) and selected only those that were furthermore consistently expressed

across different donors (r > 0.5). These genes were fed into a developmental enrichment analysis, showing strong associations with cortex, thalamus, striatum, and cerebellum during childhood-to-adulthood time window. The degree of gene expression for developmental windows is reported on the bottom. The curve represents log transformed FDR corrected p-values, averaged across the brain regions reported as on the bottom. ***FDR < 0.001, ** FDR < 0.01, *FDR < 0.05.

Association between connectome manifold and cognitive function

To finally establish associations between connectome reconfigurations and cognitive functioning, we utilized a supervised machine learning to predict full intelligence quotient (IQ) at follow-up using manifold eccentricity features. Independent variables were combinations of cortical and subcortical manifold features at baseline and their age-related trajectory data. We used elastic net regularization (Zou and Hastie, 2005) with ten-fold cross-validation (see *Methods*), and repeated the prediction 100 times with different training and test dataset compositions to mitigate subject selection bias. The manifold eccentricity of cortical regions at baseline significantly predicted future IQ score (mean ± SD r = 0.21 ± 0.03; mean absolute error (MAE) = 8.76 ± 0.10). Prediction performance was slightly improved when we combined the manifold eccentricity both at baseline and differences between follow-up and baseline (r = 0.26 ± 0.02; MAE = 8.44 ± 0.10) (**Fig. 5A**). Notably, prediction accuracy was improved if we additionally considered subcortical manifold features (baseline: r = 0.27 ± 0.02; MAE = 8.59 ± 0.12; baseline and maturational change: r = 0.34 ± 0.03; MAE = 8.74 ± 0.17) (**Fig. 5B**). The regions showing strongest predictive validity for IQ were prefrontal, parietal, and temporal cortices, as well as the caudate and thalamus. The probability map of the selected brain regions (bottom right of *Fig. 5B*) was further decoded using Neurosynth (Yarkoni et al., 2011), revealing strong associations with higher order cognitive and social terms (**Fig. S4**).

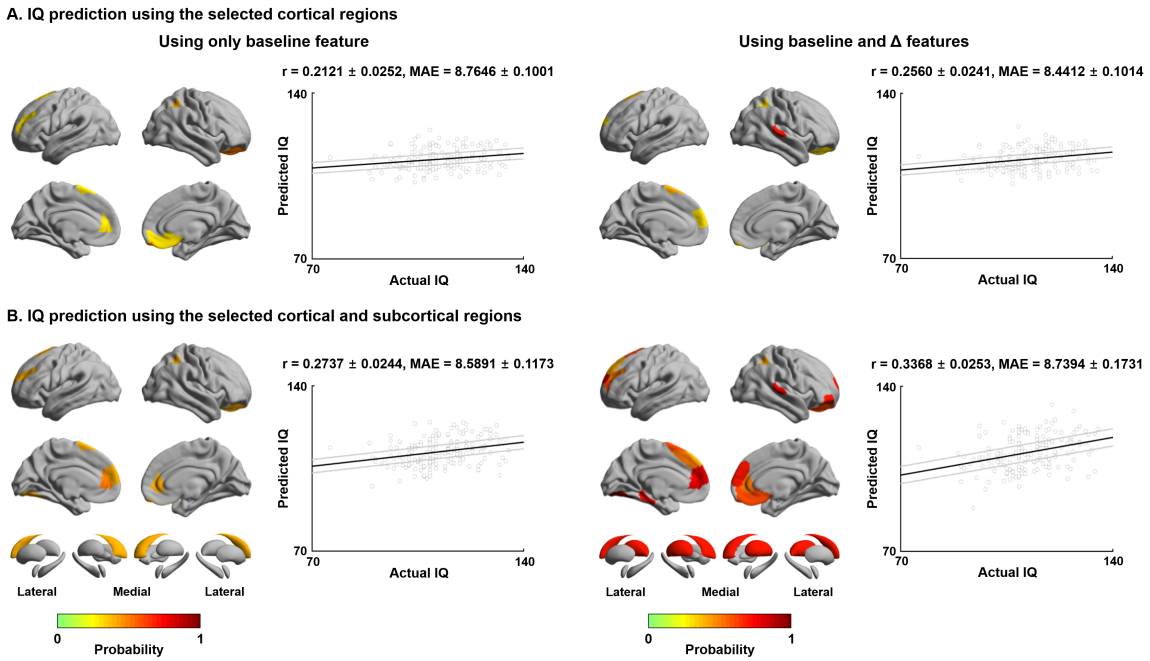

Fig. 5 | IQ prediction. (A) Probability of selected brain regions across ten-fold cross-validation and 100 repetitions for predicting future IQ using only baseline manifold eccentricity (left), and both baseline and maturational change in the feature (right). Correlations between actual and predicted IQ are reported. Black lines indicate mean correlation and gray lines represent 95% confidence interval for 100 iterations with different training/test dataset. **(B)** The prediction performance when both cortical and subcortical features were considered. *Abbreviations:* IQ, intelligence quotient; MAE, mean absolute error.

Sensitivity analysis

Repeating the longitudinal modeling with a different spatial scale (*i.e.,* 300 parcels), findings were

highly consistent (**Fig. S5**). Furthermore, manifold eccentricity of the identified cortical regions and age consistently correlated positively in the different sites and within both biological sexes, yielding non-significant interaction effects (**Fig. S6**). When we changed parameters of diffusion map embedding for generating connectome manifolds (see *Methods*), t-statistic maps of age-related changes in manifold eccentricity were largely consistent (mean ± SD linear correlation r = 0.92 ± 0.10).

DISCUSSION

The current study tracked whole-brain structural connectome maturation from adolescence to young adulthood in an accelerated longitudinal imaging cohort (Kiddle et al., 2018; Whitaker et al., 2016). Capitalizing on advanced manifold learning techniques applied to diffusion MRI derived connectomes, we established that higher order association cortices in prefrontal, medial and superior temporal, as well as parieto-occipital regions expanded in their connectome manifold representation indicative of an increased differentiation of these systems from the rest of the brain in adolescence. Parallel topological fingerprinting based on graph theory indicated that these changes co-occurred alongside increases in the within-module connectivity of transmodal cortices. Findings were consistent across the different acquisition sites and biological sexes, and similar albeit slightly weaker when correcting connectivity manifolds for MRI-based measures of cortical morphology and microstructure. In addition to the cortical manifold expansion, we found parallel reconfigurations of subcortical pathways , particularly for connectivity patterns of the caudate and thalamus. Decoding of our findings with *post-mortem* gene expression maps highlighted an implication of genes enriched in adolescence and young adulthood, again pointing to both cortical as well as subcortical targets. Finally, the combination of both cortical and subcortical manifold measures predicted behavioral measures of intelligence at follow-up, with higher performance than cortical or subcortical data alone. Collectively, our findings provide new insights into adolescent structural connectome maturation, and how multiple scales of cortical and subcortical organizations interact in typical neurodevelopment.

Leveraging advanced manifold learning, we depicted macroscale connectome organization along continuous cortical axes. Similar approaches have previously been harnessed to decompose microstructural (Paquola et al., 2019b, 2019a) and functional MRI (Bethlehem et al., 2020; Hong et al., 2019; Margulies et al., 2016; Murphy et al., 2019; Vos de Wael et al., 2020). These techniques are appealing, as they offer a low dimensional perspective on connectome reconfigurations in a data-driven and spatially unconstrained manner. In our longitudinal study, we could identify marked connectome expansion during adolescence, mainly encompassing transmodal and heteromodal association cortex in prefrontal, temporal, and posterior regions, the territories known to mature late in development (Gogtay et al., 2004; Shaw et al., 2006). Connectome expansion can be understood as an overall greater differentiation of the connectivity of these areas from the rest of the brain, as they would then cover wider portions of the corresponding manifold space. Manifold expansion in higher order areas correlated with an increase in their within-module connectivity, but not with participation coefficient and connectivity distance measures that would be more reflective of their between-module connectivity. Our findings, thus, extend prior dMRI studies that have focused on specific tract groups and that have indicated considerable developmental shifts in diffusion parameters, such as increases in fractional anisotropy and decreases in mean diffusivity in early and late adolescence (Olson et al., 2009). Other studies have furthermore reported increased streamline count estimates (Genc et al., 2020). In this context, our macroscale manifold findings likely reflect an ongoing consolidation of transmodal communities. These findings align with prior graph-theoretical studies, which have pointed to concurrent increases in network integration and

consolidation of network hubs from late childhood to early adulthood (Oldham and Fornito, 2019). Considering their distributed regional substrate, these network effects are likely driven by the ongoing maturation of fiber bundles that interconnect these higher order cortices, including superior longitudinal fascicules, but also thalamic and basal ganglia pathways (Tamnes et al., 2010), throughout adolescence.

Projecting manifold solutions back onto cortical surfaces allowed us to integrate our connectome manifold results with morphometric and intracortical intensity indices obtained via structural and quantitative MRI contrasts in the same participants. We were thus able to balance the network level effects against trajectories of intracortical remodeling. Longitudinal changes in these cortical features were overall in agreement with prior work, suggesting marked reductions in cortical thickness in adolescence (Khundrakpam et al., 2017; Shaw et al., 2006), possibly reflecting synaptic pruning processes (Petanjek et al., 2011) together with decreases in the skewness of intracortical MT profiles, a feature sensitive to preferential myelination of supragranular layers (Paquola et al., 2019a). Although we still observed significant age-related changes in manifold eccentricity after controlling for these intracortical and morphological measures, the effect sizes of our findings were reduced. This effect was particularly evident when running a parallel analysis that additionally controlled for depth dependent shifts in cortical microstructure, a finding in line with more generally demonstrated links between cortical microstructural context and inter-regional connectivity (Paquola et al., 2019b). In the context of adolescence and prior findings in the NSPN dataset (Paquola et al., 2019a), these results thus suggest a coupled process that affects depth-dependent shifts in cortical myeloarchitecture on the one hand, and adolescent shifts in macroscale connectome organization as shown by our longitudinal manifold analyses on the other.

In addition to emphasizing a distributed set of association cortices and their cortico-cortical connections, analysis of subcortico-cortical connectivity patterns highlighted parallel developmental processes in several subcortical structures and their connections, particularly the caudate and thalamus. These findings were independently supported by transcriptomic association studies and developmental enrichment analyses, which implicated genes expressed in cortical regions and these subcortical structures during late childhood, adolescence, and young adulthood. The caudate in the striatum has long been recognized to play an important role in mediating large-scale cortical network organization (Aglioti, 1997; Alexander and Crutcher, 1990; Graybiel, 1995), a finding also increasingly recognized in the connectome literature (Hwang et al., 2017; Müller et al., 2020; Shine et al., 2019). It is known to modulate activity in prefrontal association areas during memory-driven internal thought processes (Aglioti, 1997), and higher order cognitive functions, notably motivational processes, decision making, as well as cognitive control and executive functions more generally (Aglioti, 1997; Graybiel, 1995). The other structure that our analyses pointed to, striatum, participates in dense cortico-subcortical feedback loops, and exchanges neural activity through dense connections with adjacent basal ganglia structures as well as the thalamus (Aglioti, 1997; Alexander and Crutcher, 1990). These cortico-subcortical interactions likely involve the interplay of multiple neurotransmitter systems, including dopaminergic as well as GABA/Glutamate signaling. On the other hand, perturbations in cortico-striatal connections and neurotransmitter imbalances have been reported in multiple neurodevelopmental disorders, including schizophrenia (Tziortzi et al., 2014), autism (Sohal and Rubenstein, 2019), and attention deficit/hyperactivity disorder (Bonaventura et al., 2017; Hong et al., 2015).

Higher order cognitive function implicates functionally relevant whole-brain network mechanisms, and its prediction may thus leverage structurally governed principles of network integration and segregation. Application of a supervised machine learning framework with cross-validation and

regularization to our cohort demonstrated that it is possible to predict inter-individual variations in future IQ from structural connectome manifold data. These findings complement conceptual accounts linking brain organization to cognitive function (Margulies et al., 2016; Mesulam, 1998), and earlier efforts to predict IQ measures from inter-regional measures of connectivity and graph-theoretical indices of network topology (Greene et al., 2018). Notably, evaluations of several feature combinations highlighted that predictive performance was highest when including both baseline and trajectory data, and when complementing cortical and subcortical manifold features. These findings reemphasize the benefits of incorporating subcortical nodes in the characterization of large-scale cortical network organization and overall cognitive function (Alves et al., 2019; Müller et al., 2020; Shine et al., 2019).

Adolescence is a time characterized by ongoing brain changes (Baum et al., 2020; Gogtay et al., 2004; Larsen and Luna, 2018; Menon, 2013; Shaw et al., 2006), gradually increasing independence from caregivers, and strong increments in knowledge and our ability to think more abstractly and to cooperate with our peers to achieve common goals. On the other hand, adolescence is also a sensitive time window for risk taking, the development of addictions, and hosts the onset of several prevalent psychiatric disorders (Hong et al., 2019; Khundrakpam et al., 2017). Our study has shown that structural brain network organization continues to mature significantly during this time period, with particularly higher order association cortices in prefrontal and posterior regions showing an expansion of their corresponding connectome manifold signature. Findings were related to an increased strengthening of intra-community connectivity as well as cortico-subcortical connectivity patterns to thalamo-striatal regions. Although the current work was restricted to a longitudinal sample of typically developing adolescents, our framework may be useful to explore multi-scale network perturbations in cohorts with a psychiatric diagnosis or those at risk for addiction or atypical neurodevelopment.

METHODS

Participants

We obtained imaging and phenotypic data from the NSPN 2400 cohort, which contains questionnaire data on 2,402 individuals (with MRI data on a subset of ~300) from adolescence to young adulthood in a longitudinal setting (Kiddle et al., 2018; Whitaker et al., 2016). Included participants completed quality-controlled (see *Data preprocessing* section) multimodal MRI scans consisting of T1-weighted, MT, and dMRI for at least two time points. Our final sample consisted of a total of 208 participants (48% female; mean (range) age = 18.82 (14–25) years at baseline and 19.95 (15–26) at follow-up; inter-scan interval of 11.28 (6–12) months), collected from three different UK sites: Wolfson Brain Imaging Centre and MRC Cognition and Brain Sciences Unit in Cambridge; and University College London. We divided the participants into template and non-template cohorts with matched age, sex, and site ratio. The template dataset (n = 30; 50% female; mean (range) age = 18.69 (15–24) years at baseline and 19.84 ± 2.66 (16–25) at follow-up) was used for constructing template structural connectome manifold and the non-template dataset (n = 178; 47% female; mean (range) age = 18.84 (14–25) years at baseline and 19.97 (15–26) at follow-up) was used for conducting main analyses. Of note, changing the template dataset composition did not markedly affect main findings (**Fig. S7**).

MRI acquisition

Imaging data were obtained using a Siemens Magnetom TIM Trio 3T scanner. T1-weighted and MT sequences were acquired using a quantitative multiparameter mapping (MPM) sequence (repetition time (TR)/flip angle = 18.7ms/20º for T1-weighted and 23.7ms/6º for MT; six equidistance echo times (TE) = 2.2–14.7ms; voxel size = 1mm^3; 176 slices; field of view (FOV) = 256 × 240mm; matrix size = 256 × 240 × 176) (Weiskopf et al., 2013). The dMRI data were acquired using a spin-echo echo-planar imaging (EPI) sequence (TR = 8,700ms; TE = 90ms; flip angle = 90º; voxel size = 2mm^3; 70 slices; FOV = 192 × 192mm^2; matrix size = 96 × 96 × 70; b-value = 1,000s/mm^2; 63 diffusion directions; and 6 b0 images).

Data preprocessing

T1-weighted data were processed using the fusion of neuroimaging preprocessing (FuNP) pipeline integrating AFNI, FSL, FreeSurfer, ANTs, and Workbench (Avants et al., 2011; Cox, 1996; Fischl, 2012; Glasser et al., 2013; Jenkinson et al., 2012; Park et al., 2019), which is similar to the minimal preprocessing pipeline for the Human Connectome Project (Glasser et al., 2013). Gradient nonlinearity and b0 distortion correction, non-brain tissue removal, and intensity normalization were performed. The white and pial surfaces were generated by following the boundaries between different tissues (Dale et al., 1999), and they were averaged to generate the midthickness surface, which was used to generate the inflated surface. The spherical surface was registered to the Conte69 template with 164k vertices (Van Essen et al., 2012) and downsampled to a 32k vertex mesh. Quality control involved visual inspection of surface reconstruction of T1-weighted data, and cases with faulty cortical segmentation were excluded. Surface-based co-registration between T1-weighted and MT weighted scans were performed. We generated 14 equivolumetric cortical surfaces within the cortex and sampled MT intensity along these surfaces (Paquola et al., 2019a). The vertex-wise MT profiles for each surface depth were averaged based on the Schaefer atlas with 200 parcels (Schaefer et al., 2018). The dMRI data were processed using MRtrix3 (Tournier et al., 2019), including correction for susceptibility distortions, head motion, and eddy currents. We visually inspected the quality of co-registration between the adolescence data and adult-driven surface template as well as parcellation atlas, and all data showed reasonable registration results.

Structural connectome manifold identification

Structural connectomes were generated from preprocessed dMRI data (Tournier et al., 2019). Anatomically constrained tractography was performed using different tissue types derived from the T1-weighted image, including cortical and subcortical grey matter, white matter, and cerebrospinal fluid (Smith et al., 2012). Multi-shell and multi-tissue response functions were estimated (Christiaens et al., 2015), and constrained spherical-deconvolution and intensity normalization were performed (Jeurissen et al., 2014). The tractogram was generated with 40 million streamlines, with a maximum tract length of 250 and a fractional anisotropy cutoff of 0.06. Subsequently, spherical-deconvolution informed filtering of tractograms (SIFT2) was applied to reconstruct whole-brain streamlines weighted by the cross-section multipliers, which considers the fiber bundle's total intra-axonal space across its full cross-sectional extent (Smith et al., 2015). The structural connectome was built by mapping the reconstructed cross-section streamlines onto the Schaefer 7-network based atlas with 200 parcels (Schaefer et al., 2018) then log-transformed to adjust for the scale (Fornito et al., 2016).

Cortex-wide structural connectome manifolds were identified using BrainSpace

(https://github.com/MICA-MNI/BrainSpace) (Vos de Wael et al., 2020). First, a template manifold was estimated using a group representative structural connectome of the template dataset. The group representative structural connectome was defined using a distance-dependent thresholding that preserves long-range connections (Betzel et al., 2019). An affinity matrix was constructed with a kernel of normalized angle and eigenvectors were estimated via diffusion map embedding (**Fig. 1A**), which is robust to noise and computationally efficient compared to other non-linear manifold learning techniques (Tenenbaum et al., 2000). It is controlled by two parameters α and *t*, where α controls the influence of the density of sampling points on the manifold (α = 0, maximal influence; α = 1, no influence) and *t* controls the scale of eigenvalues of the diffusion operator. We set α = 0.5 and t = 0 to retain the global relations between data points in the embedded space, following prior applications (Hong et al., 2019; Margulies et al., 2016; Paquola et al., 2019a, 2019b; Vos de Wael et al., 2020). In this new manifold, interconnected brain regions are closely located, and regions with weak inter-connectivity located farther apart. After generating the template manifold, individual-level manifolds were estimated from the non-template dataset and aligned to the template manifold via Procrustes alignment (Langs et al., 2015; Vos de Wael et al., 2020). To analyze how the multi-dimensional manifold structures change in the low dimensional manifold space, we simplified the multivariate eigenvectors into a single scalar value by calculating the Euclidean distance between the center of template manifold and all data points (*i.e.,* brain regions) in the manifold space, which was referred to as manifold eccentricity (**Fig. 1B**) (Bethlehem et al., 2020). The template center was defined as the centroid of the first three eigenvectors, which explained 50% variance. Specifically, manifold eccentricity was defined as follows:

$$C_T = \frac{1}{N}\left[\sum_{i=1}^{N} T(E1)_i, \sum_{i=1}^{N} T(E2)_i, \sum_{i=1}^{N} T(E3)_i\right] \quad (1)$$

$$ME = \sqrt{\sum_{e=1}^{3}\{I(E_e) - C_T(e)\}^2} \quad (2)$$

C_T is the template center; N number of brain regions; $T(\cdot)$ template manifold; ME manifold eccentricity; $I(\cdot)$ individual manifold; $C_T(e)$ template center of eth manifold.

Age-related changes in structural manifolds

We assessed changes in manifold eccentricity across age using a linear mixed effect model (Worsley et al., 2009), controlling for effects of sex, site, head motion, and subject-specific random intercept to improve model fit in accelerated longitudinal designs. The t-statistics of each brain region were computed and we corrected for multiple comparisons by using a FDR threshold of $q < 0.05$ (**Fig. 1C**) (Benjamini and Hochberg, 1995). We stratified age-related effects based on a seminal model of neural organization and laminar differentiation that contains four cortical hierarchical levels (Mesulam, 1998), as well as seven intrinsic functional communities (Yeo et al., 2011) (**Fig. 1D**). To assess the effects with respect to age^2, we repeated implementing a linear mixed effect model by adding a quadratic term of age to the model.

To provide the underlying structure of manifold eccentricity, we compared the changes in manifold eccentricity with those in connectome topology measures. We first defined clusters within the identified regions based on their spatial boundaries (**Fig. S1A**). Then, we calculated degree centrality, as well as modular measures of within-module degree and participation coefficient using the Brain Connectivity Toolbox (https://sites.google.com/site/bctnet/) (Rubinov and Sporns, 2010) and

connectivity distance using a recently published approach (Larivière et al., 2020). Degree centrality is defined as the row-wise sum of the weighted connectivity matrix, representing the connection strength of a given node (Rubinov and Sporns, 2010). Connectivity distance is a given brain region's geodesic distance to its structurally connected brain areas within the cortex (Oligschläger et al., 2019), and it is defined as the multiplication between the geodesic distance and the binarized structural connectome (Hong et al., 2019; Oligschläger et al., 2019). Within-module degree and participation coefficient are nodal measures reflecting different facets of community organization (Rubinov and Sporns, 2010). For each individual subject, community structure was defined using Louvain's algorithm (Blondel et al., 2008) and a consistency matrix was constructed, where each element of the matrix represents whether the two different nodes are involved in the same community (*i.e.,* 1) or not (*i.e.,* 0) (**Fig. S2A**). We constructed the group-wise consistency matrix by averaging the consistency matrix of all subjects and applied k-means clustering (**Fig. S2B**). The optimal number of clusters was determined using the silhouette coefficient, *i.e.,* the k that maximized the silhouette coefficient (Kannan et al., 2010). We calculated within-module degree and participation coefficient based on these modules. Within-module degree is the degree centrality within a community, indicating intra-community connection strength, while participation coefficient represents inter-community connectivity (Rubinov and Sporns, 2010). We calculated linear correlations between changes in manifold eccentricity and those in each graph theoretical measure for each cluster (**Fig. S1B**). The significance of the correlation was corrected using 1,000 permutation tests by randomly shuffling subject indices in one of the data vectors, and we corrected for multiple comparisons across clusters using an FDR procedure (Benjamini and Hochberg, 1995). To visualize age-related changes in these parameters, we stratified each measure according to discretized age bins (< 17, 17-19, 19-21, 21-23, ≥ 23; **Fig. S3**).

Cortical morphology and microstructure

It has been shown that cortical morphology and microstructure significantly change during development (Gogtay et al., 2004; Khundrakpam et al., 2017; Paquola et al., 2019a; Shaw et al., 2006). Here, we confirmed these changes by assessing age-related changes in MRI-based cortical thickness measures and intracortical measures of MT, an index sensitive to myelin content (Weiskopf et al., 2013), using linear mixed effect models (**Fig. 2A**) (Worsley et al., 2009). We further regressed out cortical thickness and MT from the connectome manifold eccentricity metric. We then implemented linear mixed effect models using the residuals of manifold measures to assess whether age-related connectome manifold effects exist above and beyond age-related effects on cortical morphology and microstructure (**Fig. 2B**).

Subcortico-cortical connectivity

To assess age-related changes in subcortical manifold organizations in addition to cortical manifold structures, we first parcellated the accumbens, amygdala, caudate, hippocampus, pallidum, putamen, and thalamus for each individual (Patenaude et al., 2011), and approximated cross-section streamlines connect each subcortical region to the rest of the brain. For each individual and each subcortical region, we projected the streamline strength to cortical manifold space by weighting the cortical manifolds with the streamline strength of the connection between each subcortical region and cortical parcels, yielding a matrix with the form of (number of brain regions × number of cortical manifolds).

We averaged the matrix across the axis of cortical manifolds to construct subcortical-weighted manifold vector. We assessed age-related changes in the subcortical-weighted manifold using a linear mixed effect model (Worsley et al., 2009), controlling for sex, site, head motion, and subject-specific random intercept, and FDR corrected for multiple comparisons (**Fig. 3**) (Benjamini and Hochberg, 1995).

Transcriptomic analysis

We performed spatial correlation analysis to *post-mortem* gene expression data and carried out a developmental enrichment analysis (**Fig. 4**). In brief, we first correlated the t-statistics map, which represents age-related changes in manifold eccentricity that controlled for cortical morphology and microstructure, with the *post-mortem* gene expression maps provided by the Allen Institute using the Neurovault gene decoding tool (Gorgolewski et al., 2015, 2014; Hawrylycz et al., 2012). Leveraging mixed effect models to associate the input t-statistic map with the genes of six donor brains, Neurovault yields the gene symbols associated with the input spatial map. Gene symbols that passed for a significance level of FDR < 0.05 were further tested whether they are consistently expressed across different donors using abagen toolbox (https://github.com/rmarkello/abagen) (Arnatkeviciute et al., 2019). For each gene, we estimated whole-brain gene expression map and correlated it between all pairs of donors. Only genes showing consistent whole-brain expression pattern across donors (FDR < 0.05) were fed into enrichment analysis, which involved comparison against developmental expression profiles from the additional BrainSpan dataset (http://www.brainspan.org) using the cell-type specific expression analysis (CSEA) developmental expression tool (http://genetics.wustl.edu/jdlab/csea- tool-2) (Dougherty et al., 2010). As the Allen Brain Institute repository is composed of adult *post-mortem* datasets, it should be noted that the associated gene symbols represent indirect associations with the input t-statistic map derived from the developmental data.

Association with the development of cognitive function

Leveraging a supervised machine learning with ten-fold cross-validation, we predicted full IQ score measured by Wechsler Abbreviated Scale of Intelligence (Wechsler, 1999) at follow-up using cortical and subcortical features. Four different feature sets were evaluated: (1) manifold eccentricity of the identified cortical regions at baseline and (2) manifold eccentricity at baseline and its longitudinal change (*i.e.,* differences between follow-up and baseline), and (3) cortical manifold eccentricity and subcortical-weighted manifold of the identified regions at baseline and (4) manifold eccentricity and subcortical-weighted manifold at baseline and their longitudinal changes. For each evaluation, a subset of features that could predict future IQ was identified using elastic net regularization ($\rho = 0.5$) with optimized regularization parameters (L1 and L2 penalty terms) via ten-fold cross-validation (Zou and Hastie, 2005). Feature selection procedure was conducted using the training data (9/10 segments), and it was repeated 10 times with different training and test dataset. The features that were most frequently identified across the cross-validation iterations (>50%) were selected and fed into a linear regression model for predicting IQ scores. Here, the actual feature values were considered, not multiplied by the regression weights. The model was controlled for effects of age, sex, site, and head motion. The IQ prediction using linear regression was performed with a ten-fold cross-validation by training the model with the training data (9/10 segments) and applying it to the test data (1/10

segment). The prediction procedure was repeated 100 times with different training and test sets to reduce bias. Prediction accuracy was indexed by computing linear correlations between the actual and predicted IQ scores as well as mean absolute error (MAE). A 95% confidence interval of the accuracy measures was also reported. Permutation-based correlations across 1,000 tests were conducted by randomly shuffling subject indices to check whether the prediction performance exceeded chance levels.

Sensitivity analysis

a) Spatial scale. To assess the consistency of our findings across spatial scales, we additionally performed the linear mixed effect modeling using a finer parcellation scheme of 300 parcels (**Fig. S5**) (Schaefer et al., 2018).

b) Site effect. Participants were recruited from three different sites. To assess whether the longitudinal changes in manifold eccentricity across age are consistent across different sites, we calculated interaction effects of the relationship between age and manifold eccentricity of the identified regions across sites (**Fig. S6B**).

c) Sex effect. We repeated computing interaction effect of the relationship between age and manifold eccentricity across male and female subjects to assess whether the age-related changes are affected by sex (**Fig. S6C**).

d) Different parameters for diffusion map embedding. To assess the sensitivity of our findings, we generated connectome manifolds with different parameters for diffusion map embedding (α = 0.25, 0.5, 0.75; t = 0, 1, 2, 3). We assessed age-related changes of the newly defined manifold eccentricity and calculated linear correlation with t-statistic map of the default setting (α = 0.5; t = 0; *Fig. 1C*).

ACKNOWLEDGEMENTS

Dr. Bo-yong Park was funded by the National Research Foundation of Korea (NRF-2020R1A6A3A03037088), Molson Neuro-Engineering fellowship by Montreal Neurological Institute and Hospital (MNI), and a postdoctoral fellowship of the Fonds de la Recherche du Quebec – Santé (FRQ-S). Dr. Richard A. I. Bethlehem was funded by a British Academy Post-Doctoral Fellowship and the Autism Research Trust. Dr. Casey Paquola and Dr Raul R. Cruces were funded through postdoctoral fellowships of the FRQ-S. Ms. Sara Larivière acknowledges funding from the Canadian Institutes of Health Research (CIHR). Dr. Edward T. Bullmore was supported by a Senior Investigator award from the National Institute of Health Research (NIHR). Dr. Boris C. Bernhardt acknowledges research support from the National Science and Engineering Research Council of Canada (NSERC Discovery-1304413), the CIHR (FDN-154298), SickKids Foundation (NI17-039), Azrieli Center for Autism Research (ACAR-TACC), BrainCanada, FRQ-S, and the Tier-2 Canada Research Chairs program. Drs. Bo-yong Park, Richard A. I. Bethlehem, Casey Paquola, and Boris C. Bernhardt are jointly funded through an MNI-Cambridge collaborative award. The Neuroscience and Psychiatry Network (NSPN) study was funded by a Wellcome Trust award to the University of Cambridge and University College London. The data were curated and analyzed using a computational facility funded by an MRC research infra-structure award (MR/M009041/1) and supported by the NIHR Cambridge Biomedical Research Centre. The views expressed are those of the authors and not necessarily those of the NHS, the NIHR or the Department of Health and Social Care.

AUTHOR CONTRIBUTIONS

B.P. and B.C.B. designed the experiments, analyzed the data, and wrote the manuscript. R.A.I.B. aided data curation. R.A.I.B., C.P., S.L., R.R.C., and R.V.D.W. aided with the experiments. E.T.B. designed the NSPN MRI study and edited the manuscript. B.P. and B.C.B. are the corresponding authors of this work and have responsibility for the integrity of the data analysis.

CONFLICT OF INTEREST

The authors declare no conflicts of interest.

REFERENCES

Aglioti S. 1997. The role of the thalamus and basal ganglia in human cognition. *J Neurolinguistics* **10**:255–265. doi:10.1016/S0911-6044(97)00020-1

Alexander GE, Crutcher MD. 1990. Functional architecture of basal ganglia circuits: neural substrates of parallel processing. *Trends Neurosci* **13**:266–271. doi:10.1016/0166-2236(90)90107-L

Alves PN, Foulon C, Karolis V, Bzdok D, Margulies DS, Volle E, Thiebaut de Schotten M. 2019. An improved neuroanatomical model of the default-mode network reconciles previous neuroimaging and neuropathological findings. *Commun Biol* **2**:370. doi:10.1038/s42003-019-0611-3

Arnatkeviciute A, Fulcher BD, Fornito A. 2019. A practical guide to linking brain-wide gene expression and neuroimaging data. *Neuroimage* **189**:353–367. doi:10.1016/j.neuroimage.2019.01.011

Avants BB, Tustison NJ, Song G, Cook PA, Klein A, Gee JC. 2011. A reproducible evaluation of ANTs similarity metric performance in brain image registration. *Neuroimage* **54**:2033–2044. doi:10.1016/j.neuroimage.2010.09.025

Baum GL, Cui Z, Roalf DR, Ciric R, Betzel RF, Larsen B, Cieslak M, Cook PA, Xia CH, Moore TM, Ruparel K, Oathes DJ, Alexander-Bloch AF, Shinohara RT, Raznahan A, Gur RE, Gur RC, Bassett DS, Satterthwaite TD. 2020. Development of structure–function coupling in human brain networks during youth. *Proc Natl Acad Sci U S A* **117**:771–778. doi:10.1073/pnas.1912034117

Benjamini Y, Hochberg Y. 1995. Controlling the False Discovery Rate : A Practical and Powerful Approach to Multiple Testing. *J R Stat Soc* **57**:289–300.

Bethlehem RAI, Paquola C, Seidlitz J, Ronan L, Bernhardt B, Consortium CCAN, Tsvetanov KA. 2020. Dispersion of functional gradients across the adult lifespan. *Neuroimage* **222**:117299. doi:10.1016/j.neuroimage.2020.117299

Betzel RF, Griffa A, Hagmann P, Miši´c B. 2019. Distance-dependent consensus thresholds for generating group-representative structural brain networks. *Netw Neurosci* **3**:475–496. doi:10.1162/netn_a_00075

Blondel VD, Guillaume JL, Lambiotte R, Lefebvre E. 2008. Fast unfolding of communities in large networks. *J Stat Mech Theory Exp* **2008**. doi:10.1088/1742-5468/2008/10/P10008

Bonaventura J, Quiroz C, Cai NS, Rubinstein M, Tanda G, Ferré S. 2017. Key role of the dopamine D4 receptor in the modulation of corticostriatal glutamatergic neurotransmission. *Sci Adv* **3**:e1601631. doi:10.1126/sciadv.1601631

Buckner RL, Krienen FM. 2013. The evolution of distributed association networks in the human brain. *Trends Cogn Sci* **17**:648–665. doi:10.1016/j.tics.2013.09.017

Christiaens D, Reisert M, Dhollander T, Sunaert S, Suetens P, Maes F. 2015. Global tractography of multi-shell diffusion-weighted imaging data using a multi-tissue model. *Neuroimage* **123**:89–101. doi:10.1016/j.neuroimage.2015.08.008

Cox RW. 1996. AFNI : Software for Analysis and Visualization of Functional Magnetic Resonance Neuroimages. *Comput Biomed Res* **29**:162–173. doi:10.1006/cbmr.1996.0014

Dale AM, Fischl B, Sereno MI. 1999. Cortical surface-based analysis: I. Segmentation and surface

reconstruction. *Neuroimage* **9**:179–194. doi:10.1006/nimg.1998.0395

Dougherty JD, Schmidt EF, Nakajima M, Heintz N. 2010. Analytical approaches to RNA profiling data for the identification of genes enriched in specific cells. *Nucleic Acids Res* **38**:4218–4230. doi:10.1093/nar/gkq130

Fischl B. 2012. FreeSurfer. *Neuroimage* **62**:774–781. doi:10.1016/j.neuroimage.2012.01.021

Fornito A, Arnatkevičiūtė A, Fulcher BD. 2019. Bridging the Gap between Connectome and Transcriptome. *Trends Cogn Sci* **23**:34–50. doi:10.1016/j.tics.2018.10.005

Fornito A, Zalesky A, Bullmore E. 2016. Fundamentals of Brain Network Analysis. Amsterdam: Academic Press.

Genc S, Malpas CB, Gulenc A, Sciberras E, Efron D, Silk TJ, Seal ML. 2020. Longitudinal white matter development in children is associated with puberty, attentional difficulties, and mental health. *bioRxiv*. doi:10.1101/607671

Glasser MF, Sotiropoulos SN, Wilson JA, Coalson TS, Fischl B, Andersson JL, Xu J, Jbabdi S, Webster M, Polimeni JR, Van Essen DC, Jenkinson M. 2013. The minimal preprocessing pipelines for the Human Connectome Project. *Neuroimage* **80**:105–124. doi:10.1016/j.neuroimage.2013.04.127

Gogtay N, Giedd JN, Lusk L, Hayashi KM, Greenstein D, Vaituzis AC, Nugent TF, Herman DH, Clasen LS, Toga AW, Rapoport JL, Thompson PM. 2004. Dynamic mapping of human cortical development during childhood through early adulthood. *Proc Natl Acad Sci U S A* **101**:8174–8179. doi:10.1073/pnas.0402680101

Gorgolewski KJ, Fox AS, Chang L, Schäfer A, Arélin K, Burmann I, Sacher J, Margulies DS. 2014. Tight fitting genes: finding relations between statistical maps and gene expression patternsF1000Posters. p. 1607 (Poster).

Gorgolewski KJ, Varoquaux G, Rivera G, Schwarz Y, Ghosh SS, Maumet C, Sochat V V., Nichols TE, Poldrack RA, Poline JB, Yarkoni T, Margulies DS. 2015. NeuroVault.Org: A web-based repository for collecting and sharing unthresholded statistical maps of the human brain. *Front Neuroinform* **9**:Article 8. doi:10.3389/fninf.2015.00008

Graybiel AM. 1995. Building action repertoires: memory and learning functions of the basal ganglia. *Curr Opin Neurobiol* **5**:733–741. doi:10.1016/0959-4388(95)80100-6

Greene AS, Gao S, Scheinost D, Constable RT, Greene A. 2018. Task-induced brain state manipulation improves prediction of individual traits. *Nat Commun* **9**:2807. doi:10.1038/s41467-018-04920-3

Hagmann P, Sporns O, Madan N, Cammoun L, Pienaar R, Wedeen VJ, Meuli R, Thiran JP, Grant PE. 2010. White matter maturation reshapes structural connectivity in the late developing human brain. *Proc Natl Acad Sci U S A* **107**:19067–19072. doi:10.1073/pnas.1009073107

Hawrylycz MJ, Lein ES, Guillozet-Bongaarts AL, Shen EH, Ng L, Miller JA, van de Lagemaat LN, Smith KA, Ebbert A, Riley ZL, Abajian C, Beckmann CF, Bernard A, Bertagnolli D, Boe AF, Cartagena PM, Mallar Chakravarty M, Chapin M, Chong J, Dalley RA, Daly BD, Dang C, Datta S, Dee N, Dolbeare TA, Faber V, Feng D, Fowler DR, Goldy J, Gregor BW, Haradon Z, Haynor DR, Hohmann JG, Horvath S, Howard RE, Jeromin A, Jochim JM, Kinnunen M, Lau C, Lazarz ET, Lee C, Lemon TA, Li L, Li Y, Morris JA, Overly CC, Parker PD, Parry SE, Reding M, Royall JJ, Schulkin J, Sequeira PA, Slaughterbeck CR, Smith SC, Sodt AJ, Sunkin SM, Swanson BE, Vawter MP, Williams D, Wohnoutka P, Ronald Zielke H, Geschwind DH, Hof PR, Smith SM, Koch C, Grant SGN, Jones AR. 2012. An anatomically comprehensive

atlas of the adult human brain transcriptome. *Nature* **489**:391–399. doi:10.1038/nature11405

Herting MM, Johnson C, Mills KL, Vijayakumar N, Dennison M, Liu C, Goddings AL, Dahl RE, Sowell ER, Whittle S, Allen NB, Tamnes CK. 2018. Development of subcortical volumes across adolescence in males and females: A multisample study of longitudinal changes. *Neuroimage* **172**:194–205. doi:10.1016/j.neuroimage.2018.01.020

Hong S-J, Vos De Wael R, Bethlehem RAI, Lariviere S, Paquola C, Valk SL, Milham MP, Martino A Di, Margulies DS, Smallwood J, Bernhardt BC. 2019. Atypical functional connectome hierarchy in autism. *Nat Commun* **10**:1022.

Hong SB, Harrison BJ, Fornito A, Sohn CH, Song IC, Kim JW. 2015. Functional dysconnectivity of corticostriatal circuitry and differential response to methylphenidate in youth with attention-deficit/hyperactivity disorder. *J Psychiatry Neurosci* **40**:46–57. doi:10.1503/jpn.130290

Hwang K, Bertolero MA, Liu WB, D'Esposito M. 2017. The human thalamus is an integrative hub for functional brain networks. *J Neurosci* **37**:5594–5607. doi:10.1523/JNEUROSCI.0067-17.2017

Jenkinson M, Beckmann CF, Behrens TEJ, Woolrich MW, Smith SM. 2012. Fsl. *Neuroimage* **62**:782–790. doi:10.1016/j.neuroimage.2011.09.015

Jeurissen B, Tournier JD, Dhollander T, Connelly A, Sijbers J. 2014. Multi-tissue constrained spherical deconvolution for improved analysis of multi-shell diffusion MRI data. *Neuroimage* **103**:411–426. doi:10.1016/j.neuroimage.2014.07.061

Kannan SR, Ramathilagam S, Sathya A, Pandiyarajan R. 2010. Effective fuzzy c-means based kernel function in segmenting medical images. *Comput Biol Med* **40**:572–579. doi:10.1016/j.compbiomed.2010.04.001

Karapanagiotidis T, Vidaurre D, Quinn AJ, Vatansever D, Poerio GL, Turnbull A, Siu N, Ho P, Leech R, Bernhardt BC, Jefferies E, Margulies DS, Nichols TE, Woolrich MW, Smallwood J. 2020. The psychological correlates of distinct neural states occurring during wakeful rest. *bioRxiv*. doi:10.1101/2019.12.21.885772

Khundrakpam BS, Lewis JD, Kostopoulos P, Carbonell F, Evans AC. 2017. Cortical Thickness Abnormalities in Autism Spectrum Disorders Through Late Childhood, Adolescence, and Adulthood: A Large-Scale MRI Study. *Cereb cortex* **27**:1721–1731. doi:10.1093/cercor/bhx038

Kiddle B, Inkster B, Prabhu G, Moutoussis M, Whitaker KJ, Bullmore ET, Dolan RJ, Fonagy P, Goodyer IM, Jones PB, Dolan R, Hauser T, Vértes P, Whitaker K, Villis L, Bhatti J, Ooi C, Widmer B, Alrumaithi A, Birt S, Cleridou K, Dadabhoy H, Granville S, Harding E, Hopkins A, Isaacs D, King J, Kokorikou D, Mills H, O'Donnell C, Pantaleone S, Dyan P, Fearon P, Kievit R, Stochl J, van Harmelen AL. 2018. Cohort profile: The NSPN 2400 Cohort: A developmental sample supporting the Wellcome Trust Neuro Science in Psychiatry Network. *Int J Epidemiol* **47**:18-19g. doi:10.1093/ije/dyx117

Langs G, Golland P, Ghosh SS. 2015. Predicting Activation Across Individuals with Resting-State Functional Connectivity Based Multi-Atlas Label FusionInternational Conference on Medical Image Computing and Computer-Assisted Intervention. pp. 313–320. doi:10.1007/978-3-319-24571-3_38

Larivière S, Weng Y, Vos de Wael R, Royer J, Frauscher B, Wang Z, Bernasconi A, Bernasconi N, Schrader D V., Zhang Z, Bernhardt BC. 2020. Functional connectome contractions in temporal lobe epilepsy: Microstructural underpinnings and predictors of surgical outcome. *Epilepsia*

61:1221–1233. doi:10.1111/epi.16540

Larsen B, Luna B. 2018. Adolescence as a neurobiological critical period for the development of higher-order cognition. *Neurosci Biobehav Rev* **94**:179–195. doi:10.1016/j.neubiorev.2018.09.005

Lebel C, Beaulieu C. 2011. Longitudinal development of human brain wiring continues from childhood into adulthood. *J Neurosci* **31**:10937–10947. doi:10.1523/JNEUROSCI.5302-10.2011

Louis TA, Robins J, Dockery DW, Spiro A, Ware JH. 1986. Explaining discrepancies between longitudinal and cross-sectional models. *J Chronic Dis* **39**:831–839. doi:10.1016/0021-9681(86)90085-8

Margulies DS, Ghosh SS, Goulas A, Falkiewicz M, Huntenburg JM, Langs G, Bezgin G, Eickhoff SB, Castellanos FX, Petrides M, Jefferies E, Smallwood J. 2016. Situating the default-mode network along a principal gradient of macroscale cortical organization. *Proc Natl Acad Sci U S A* **113**:12574–12579. doi:10.1073/pnas.1608282113

Markello R, Shafiei G, Zheng Y-Q, Mišić B. 2020. abagen: A toolbox for the Allen Brain Atlas genetics data. *Zenodo*. doi:http://doi.org/10.5281/zenodo.4091537

Mckeown B, Strawson WH, Wang HT, Karapanagiotidis T, Vos de Wael R, Benkarim O, Turnbull A, Margulies D, Jefferies E, McCall C, Bernhardt B, Smallwood J. 2020. The relationship between individual variation in macroscale functional gradients and distinct aspects of ongoing thought. *Neuroimage* **220**:117072. doi:10.1016/j.neuroimage.2020.117072

Menon V. 2013. Developmental pathways to functional brain networks: Emerging principles. *Trends Cogn Sci* **17**:627–640. doi:10.1016/j.tics.2013.09.015

Mesulam MM. 1998. From sensation to cognition. *Brain* **121**:1013–1052. doi:10.1093/brain/121.6.1013

Müller EJ, Munn B, Hearne LJ, Smith JB, Fulcher B, Arnatkevičiūtė A, Lurie DJ, Cocchi L, Shine JM. 2020. Core and matrix thalamic sub-populations relate to spatio-temporal cortical connectivity gradients. *Neuroimage* **222**:117224. doi:10.1016/j.neuroimage.2020.117224

Murphy C, Wang HT, Konu D, Lowndes R, Margulies DS, Jefferies E, Smallwood J. 2019. Modes of operation: A topographic neural gradient supporting stimulus dependent and independent cognition. *Neuroimage* **186**:487–496. doi:10.1016/j.neuroimage.2018.11.009

Oldham S, Fornito A. 2019. The development of brain network hubs. *Dev Cogn Neurosci* **36**:100607. doi:10.1016/j.dcn.2018.12.005

Oligschläger S, Xu T, Baczkowski BM, Falkiewicz M, Falchier A, Linn G, Margulies DS. 2019. Gradients of connectivity distance in the cerebral cortex of the macaque monkey. *Brain Struct Funct* **224**:925–935. doi:10.1007/s00429-018-1811-1

Olson EA, Collins PF, Hooper CJ, Muetzel R, Lim KO, Luciana M. 2009. White matter integrity predicts delay discounting behavior in 9- to 23-year-olds: A diffusion tensor imaging study. *J Cogn Neurosci* **21**:1406–1421. doi:10.1162/jocn.2009.21107

Paquola C, Bethlehem RA, Seidlitz J, Wagstyl K, Romero-Garcia R, Whitaker KJ, Vos de Wael R, Williams GB, Vértes PE, Margulies DS, Bernhardt B, Bullmore ET. 2019a. Shifts in myeloarchitecture characterise adolescent development of cortical gradients. *Elife* **8**:1–23. doi:10.7554/eLife.50482

Paquola C, Vos De Wael R, Wagstyl K, Bethlehem RAI, Hong SJ, Seidlitz J, Bullmore ET, Evans AC, Misic B, Margulies DS, Smallwood J, Bernhardt BC. 2019b. Microstructural and functional gradients are increasingly dissociated in transmodal cortices. *PLoS Biol* **17**:e3000284. doi:10.1371/journal.pbio.3000284

Park B, Byeon K, Park H. 2019. FuNP (Fusion of Neuroimaging Preprocessing) Pipelines: A Fully Automated Preprocessing Software for Functional Magnetic Resonance Imaging. *Front Neuroinform* **13**:5. doi:10.3389/fninf.2019.00005

Park B, Vos de Wael R, Paquola C, Larivière S, Benkarim O, Royer J, Tavakol S, Cruces RR, Li Q, Valk SL, Margulies DS, Mišić B, Bzdok D, Smallwood J, Bernhardt BC. 2021. Signal diffusion along connectome gradients and inter-hub routing differentially contribute to dynamic human brain function. *Neuroimage* **224**:117429. doi:10.1016/j.neuroimage.2020.117429

Patenaude B, Smith SM, Kennedy DN, Jenkinson M. 2011. A Bayesian model of shape and appearance for subcortical brain segmentation. *Neuroimage* **56**:907–922. doi:10.1016/j.neuroimage.2011.02.046

Petanjek Z, Judaš M, Šimić G, Rašin MR, Uylings HBM, Rakic P, Kostović I. 2011. Extraordinary neoteny of synaptic spines in the human prefrontal cortex. *Proc Natl Acad Sci U S A* **108**:13281–13286. doi:10.1073/pnas.1105108108

Rubinov M, Sporns O. 2010. Complex network measures of brain connectivity: uses and interpretations. *Neuroimage* **52**:1059–1069. doi:10.1016/j.neuroimage.2009.10.003

Schaefer A, Kong R, Gordon EM, Laumann TO, Zuo X-N, Holmes AJ, Eickhoff SB, Yeo BTT. 2018. Local-Global Parcellation of the Human Cerebral Cortex from Intrinsic Functional Connectivity MRI. *Cereb Cortex* **28**:3095–3114. doi:10.1093/cercor/bhx179

Schmithorst VJ, Yuan W. 2010. White matter development during adolescence as shown by diffusion MRI. *Brain Cogn* **72**:16–25. doi:10.1016/j.bandc.2009.06.005

Shaw P, Greenstein D, Lerch J, Clasen L, Lenroot R, Gogtay N, Evans A, Rapoport J, Giedd J. 2006. Intellectual ability and cortical development in children and adolescents. *Nature* **440**:676–679. doi:10.1038/nature04513

Shine JM, Hearne LJ, Breakspear M, Hwang K, Müller EJ, Sporns O, Poldrack RA, Mattingley JB, Cocchi L. 2019. The Low-Dimensional Neural Architecture of Cognitive Complexity Is Related to Activity in Medial Thalamic Nuclei. *Neuron* **104**:849-855.e3. doi:10.1016/j.neuron.2019.09.002

Smith RE, Tournier JD, Calamante F, Connelly A. 2015. SIFT2: Enabling dense quantitative assessment of brain white matter connectivity using streamlines tractography. *Neuroimage* **119**:338–351. doi:10.1016/j.neuroimage.2015.06.092

Smith RE, Tournier JD, Calamante F, Connelly A. 2012. Anatomically-constrained tractography: Improved diffusion MRI streamlines tractography through effective use of anatomical information. *Neuroimage* **62**:1924–1938. doi:10.1016/j.neuroimage.2012.06.005

Sohal VS, Rubenstein JLR. 2019. Excitation-inhibition balance as a framework for investigating mechanisms in neuropsychiatric disorders. *Mol Psychiatry* **24**:1248–1257. doi:10.1038/s41380-019-0426-0

Tamnes CK, Herting MM, Goddings AL, Meuwese R, Blakemore SJ, Dahl RE, Güroğlu B, Raznahan A, Sowell ER, Crone EA, Mills KL. 2017. Development of the cerebral cortex across adolescence: A multisample study of inter-related longitudinal changes in cortical

volume, surface area, and thickness. *J Neurosci* **37**:3402–3412. doi:10.1523/JNEUROSCI.3302-16.2017

Tamnes CK, Østby Y, Fjell AM, Westlye LT, Due-Tønnessen P, Walhovd KB. 2010. Brain maturation in adolescence and young adulthood: Regional age-related changes in cortical thickness and white matter volume and microstructure. *Cereb Cortex* **20**:534–548. doi:10.1093/cercor/bhp118

Tenenbaum JB, Silva V de, Langford JC. 2000. A Global Geometric Framework for Nonlinear Dimensionality Reduction. *Science (80-)* **290**:2319–2323. doi:10.1126/science.290.5500.2319

Tournier JD, Smith R, Raffelt D, Tabbara R, Dhollander T, Pietsch M, Christiaens D, Jeurissen B, Yeh CH, Connelly A. 2019. MRtrix3: A fast, flexible and open software framework for medical image processing and visualisation. *Neuroimage* **202**:116137. doi:10.1016/j.neuroimage.2019.116137

Tziortzi AC, Haber SN, Searle GE, Tsoumpas C, Long CJ, Shotbolt P, Douaud G, Jbabdi S, Behrens TEJ, Rabiner EA, Jenkinson M, Gunn RN. 2014. Connectivity-based functional analysis of dopamine release in the striatum using diffusion-weighted MRI and positron emission tomography. *Cereb Cortex* **24**:1165–1177. doi:10.1093/cercor/bhs397

Valk SL, Xu T, Margulies DS, Masouleh SK, Paquola C, Goulas A, Kochunov P, Smallwood J, Yeo BTT, Bernhardt BC, Eickhoff SB. 2020. Shaping brain structure: Genetic and phylogenetic axes of macroscale organization of cortical thickness. *Sci Adv* **6**:1–15. doi:10.1126/sciadv.abb3417

Van Essen DC, Glasser MF, Dierker DL, Harwell J, Coalson T. 2012. Parcellations and hemispheric asymmetries of human cerebral cortex analyzed on surface-based atlases. *Cereb cortex* **22**:2241–2262. doi:10.1093/cercor/bhr291

Váša F, Romero-Garcia R, Kitzbichler MG, Seidlitz J, Whitaker KJ, Vaghi MM, Kundu P, Patel AX, Fonagy P, Dolan RJ, Jones PB, Goodyer IM, Vértes PE, Bullmore ET. 2020. Conservative and disruptive modes of adolescent change in human brain functional connectivity. *Proc Natl Acad Sci U S A* **117**:3248–3253. doi:10.1073/pnas.1906144117

Vos de Wael R, Benkarim O, Paquola C, Lariviere S, Royer J, Tavakol S, Xu T, Hong S-J, Valk SL, Misic B, Milham MP, Margulies DS, Smallwood J, Bernhardt BC. 2020. BrainSpace: a toolbox for the analysis of macroscale gradients in neuroimaging and connectomics datasets. *Commun Biol* **3**:103. doi:10.1038/s42003-020-0794-7

Wechsler D. 1999. Wechsler Abbreviated Scales of Intelligence (WASI). San Antonio, TX: Psychological Corporation.

Weiskopf N, Suckling J, Williams G, Correia M. MM, Inkster B, Tait R, Ooi C, Bullmore T. ET, Lutti A. 2013. Quantitative multi-parameter mapping of R1, PD*, MT, and R2* at 3T: A multi-center validation. *Front Neurosci* **7**:95. doi:10.3389/fnins.2013.00095

Whitaker KJ, Vértes PE, Romero-Garciaa R, Váša F, Moutoussis M, Prabhu G, Weiskopf N, Callaghan MF, Wagstyl K, Rittman T, Tait R, Ooi C, Suckling J, Inkster B, Fonagy P, Dolan RJ, Jones PB, Goodyer IM, Bullmore ET. 2016. Adolescence is associated with genomically patterned consolidation of the hubs of the human brain connectome. *Proc Natl Acad Sci U S A* **113**:9105–9110. doi:10.1073/pnas.1601745113

Worsley KJ, Taylor JE, Carbonell, Chung MK, Duerden E, Bernhardt B, Lyttelton O, Boucher M, Evans AC. 2009. SurfStat: A Matlab toolbox for the statistical analysis of univariate and multivariate surface and volumetric data using linear mixed effects models and random field

theory. *Neuroimage* **47**:S102. doi:10.1016/S1053-8119(09)70882-1

Yarkoni T, Poldrack RA, Nichols TE, Van Essen DC, Wager TD. 2011. Large-scale automated synthesis of human functional neuroimaging data. *Nat Methods* **8**:665–670. doi:10.1038/nmeth.1635

Yeo BTT, Krienen FM, Sepulcre J, Sabuncu MR, Lashkari D, Hollinshead M, Roffman JL, Smoller JW, Zollei L, Polimeni JR, Fischl B, Liu H, Buckner RL. 2011. The organization of the human cerebral cortex estimated by intrinsic functional connectivity. *J Neurophysiol* **106**:1125–1165. doi:10.1152/jn.00338.2011.

Zou H, Hastie T. 2005. Regularization and variable selection via the Elastic Net. *J R Stat Soc Ser B* **67**:301–320. doi:10.1111/j.1467-9868.2005.00503.x

Supporting Information

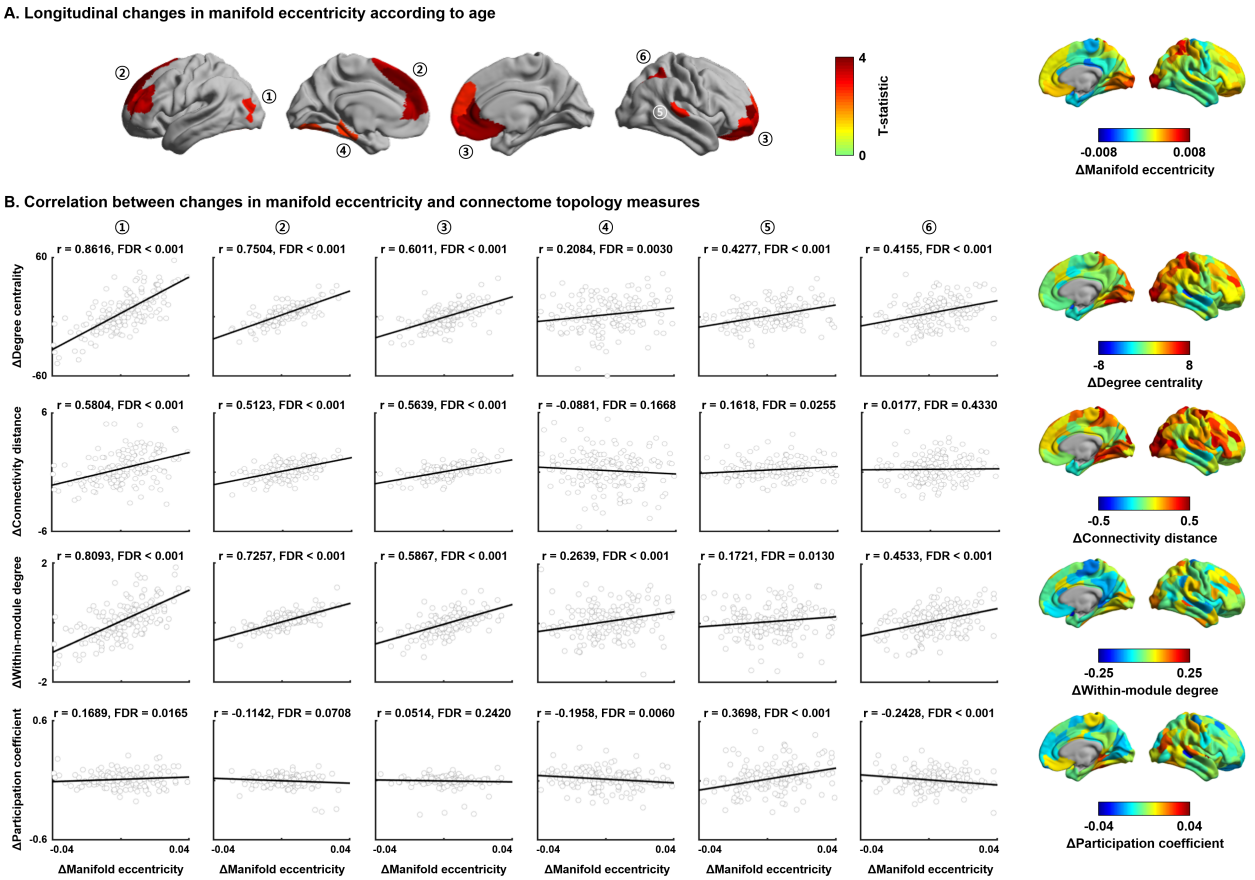

Fig. S1 | Association between structural connectome manifold and connectome topology measures. (A) Six clusters defined within the identified regions that showed significant age-related changes in manifold eccentricity (see *Fig. 1C*). **(B)** Associations between within-subject changes in manifold eccentricity and those of each connectome topology measure. Brain surfaces on the right side represent changes in each measure between baseline and follow-up. Significance was calculated using a false discovery rate (FDR).

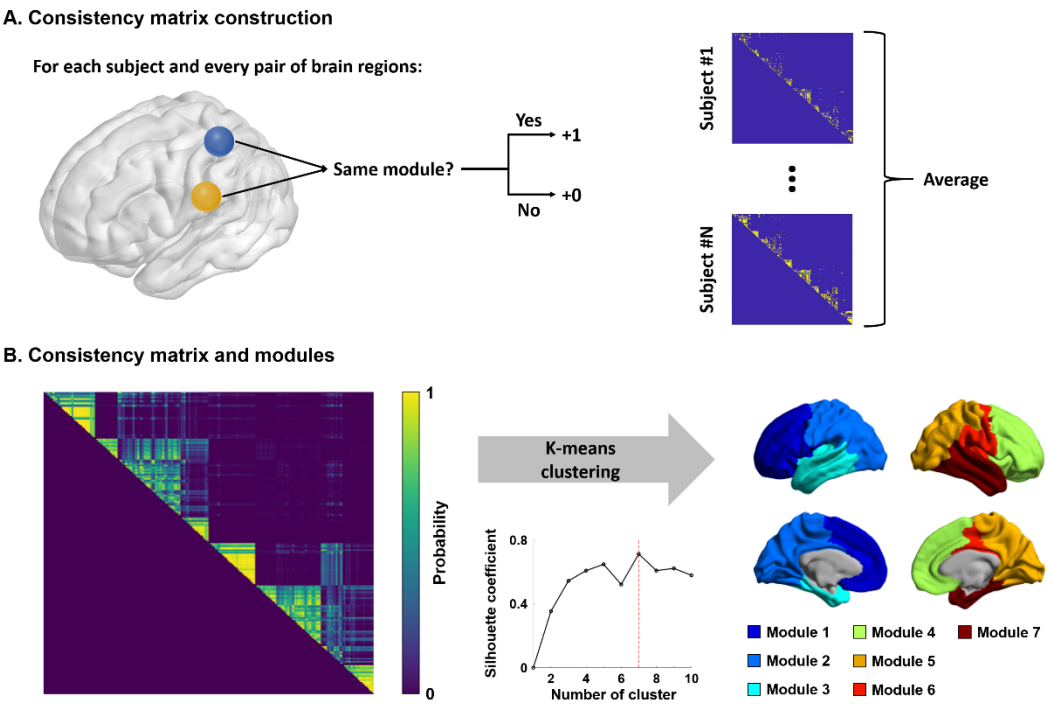

Fig. S2 | Modular structures. (A) Pipeline for constructing consistency matrix. We constructed individual subject-wise consistency matrix by considering whether two different nodes were involved in the same module. **(B)** Group-wise consistency matrix was constructed by averaging subject-wise consistency matrices. The k-means clustering with silhouette coefficient was used for defining modules. Seven modules on the brain surface are reported on the right side.

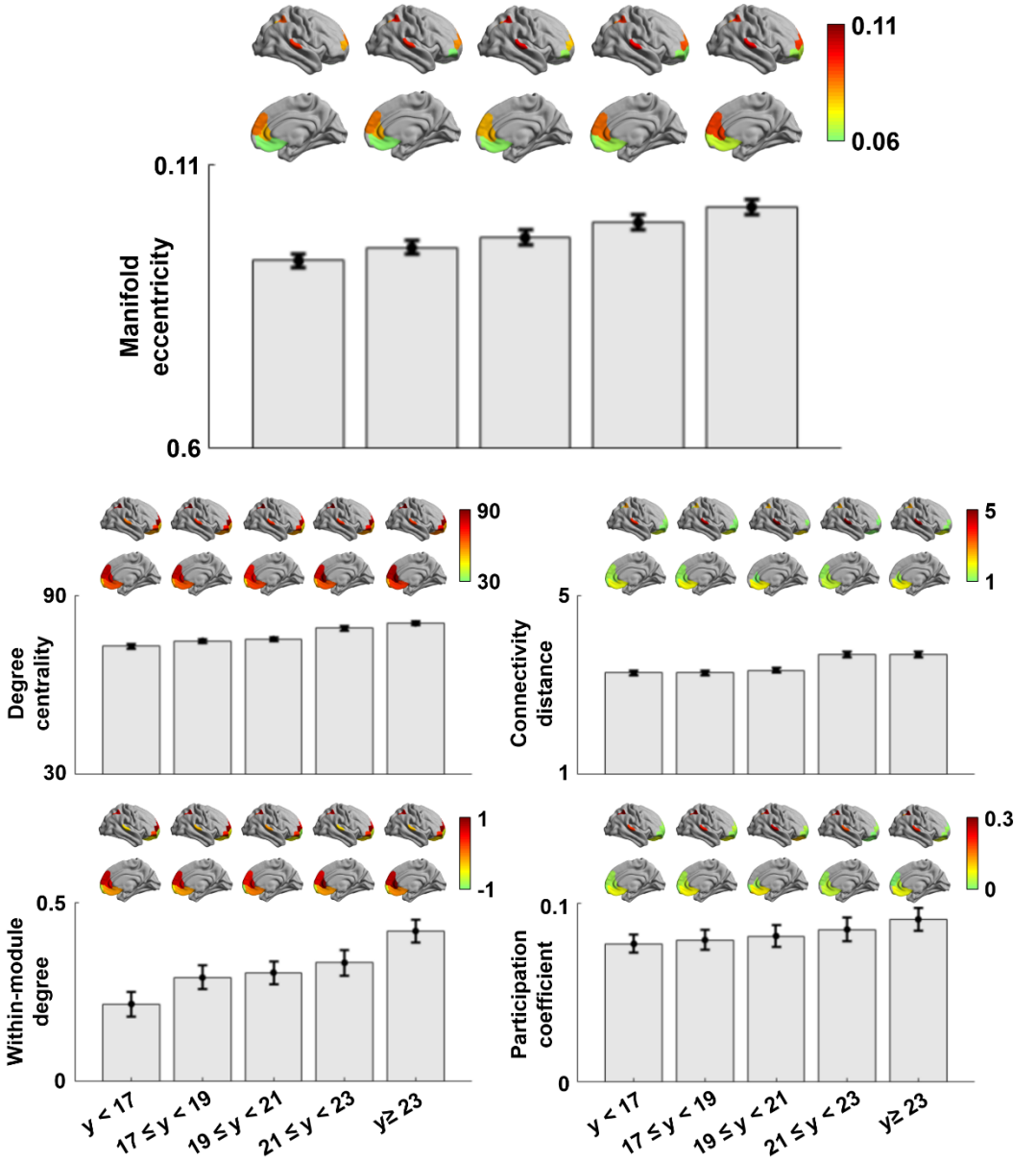

Fig. S3 | Age-related trends in connectome topology measures. Age-related changes in manifold eccentricity, degree centrality, connectivity distance, within-module degree, and participation coefficient. *Abbreviation:* y, years.

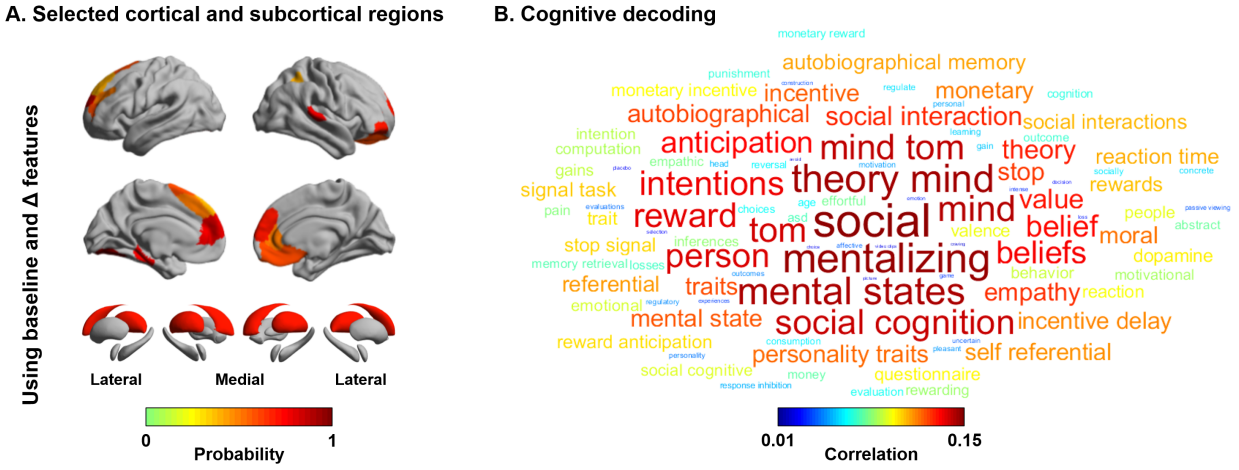

Fig. S4 | Cognitive decoding of the selected regions for IQ prediction. (A) Probability of selected cortical and subcortical regions for predicting future IQ using both baseline and maturational changes (see *Fig. 5*). **(B)** A word cloud derived by cognitive decoding using NeuroSynth (Yarkoni et al., 2011).

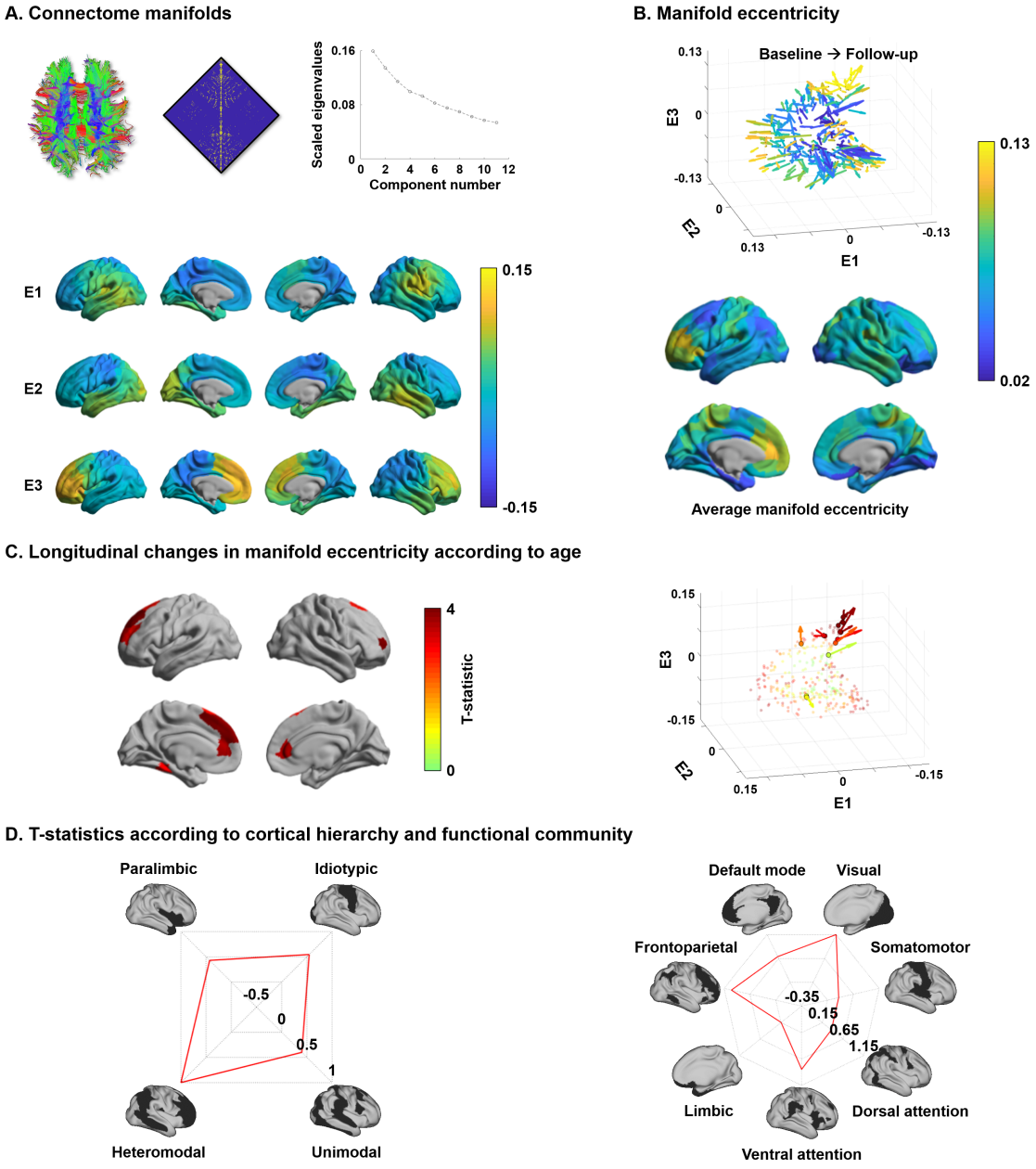

Fig. S5 | Structural connectome manifolds using Schaefer 300 atlas. (A-D) Main findings were replicated using a different parcellation scale. For details, see *Fig. 1*.

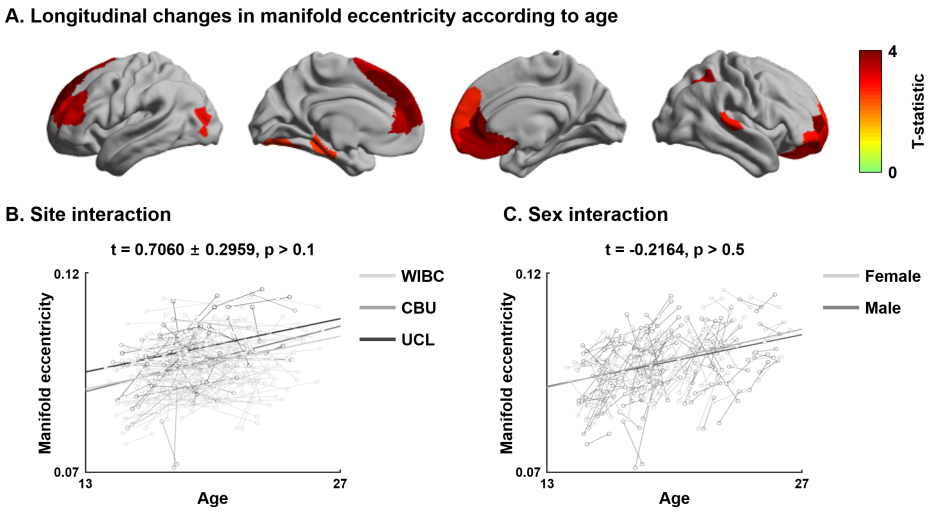

Fig. S6 | Sensitivity analysis for site and sex. (A) The t-statistics of identified regions that showed significant age-related changes in manifold eccentricity. **(B)** Interaction effects of the relationship between age and manifold eccentricity for sites and **(C)** biological sexes. *Abbreviations:* WIBC, Wolfson Brain Imaging Centre; CBU, MRC Cognition and Brain Sciences Unit; UCL, University College London.

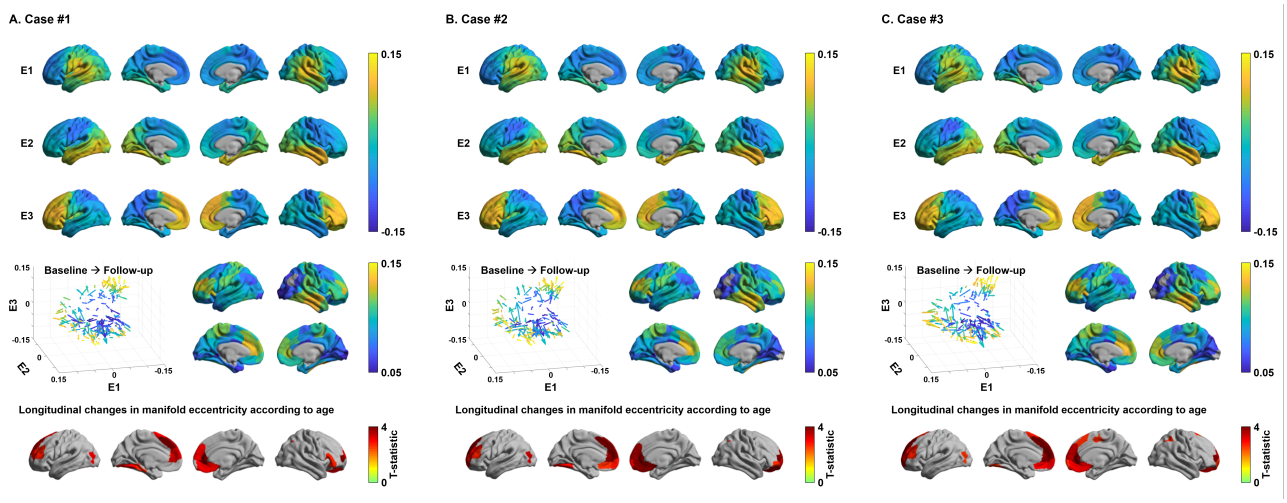

Fig. S7 | Structural connectome manifolds using different template dataset. (A-C) Structural connectome manifolds and association to age using different template cohort. Three representative cases are reported. For details, see *Figure 1*.

Data S1 | Significant gene lists correlated with patterns of manifold eccentricity changes across age. Gene symbol with name and t-statistic as well as false discover rate (FDR) corrected p-value are reported in the Supplementary Data file (Supplementary_Data1.xlsx).

Neuroscience in Psychiatry Network (NSPN) Consortium author list

Principal investigators:
Edward Bullmore (CI from 01/01/2017)[1,2,3]; Raymond Dolan[4,5]; Ian Goodyer (CI until 01/01/2017)[1]; Peter Fonagy[6]; Peter Jones[1]

NSPN (funded) staff:
Michael Moutoussis[4,5]; Tobias Hauser[4,5]; Sharon Neufeld[1]; Rafael Romero-Garcia[1,2]; Michelle St Clair[1]; Petra Vértes[1,2]; Kirstie Whitaker[1,2]; Becky Inkster[1]; Gita Prabhu[4,5]; Cinly Ooi[1]; Umar Toseeb[1]; Barry Widmer[1]; Junaid Bhatti[1]; Laura Villis[1]; Ayesha Alrumaithi[1]; Sarah Birt[1]; Aislinn Bowler[5]; Kalia Cleridou[5]; Hina Dadabhoy[5]; Emma Davies[1]; Ashlyn Firkins[1]; Sian Granville[5]; Elizabeth Harding[5]; Alexandra Hopkins[4,5]; Daniel Isaacs[5]; Janchai King[5]; Danae Kokorikou[5,6]; Christina Maurice[1]; Cleo McIntosh[1]; Jessica Memarzia[1]; Harriet Mills[5]; Ciara O'Donnell[1]; Sara Pantaleone[5]; Jenny Scott[1]; Beatrice Kiddle[1]; Ela Polek[1]

Affiliated scientists:
Pasco Fearon[6]; John Suckling[1]; Anne-Laura van Harmelen[1]; Rogier Kievit[4,7]; Sam Chamberlain[1]

[1]*Department of Psychiatry, University of Cambridge, United Kingdom*
[2]*Behavioural and Clinical Neuroscience Institute, University of Cambridge, United Kingdom*
[3]*ImmunoPsychiatry, GlaxoSmithKline Research and Development, United Kingdom*
[4]*Max Planck University College London Centre for Computational Psychiatry and Ageing Research, University College London, UK*
[5]*Wellcome Centre for Human Neuroimaging, University College London, United Kingdom*
[6]*Research Department of Clinical, Educational and Health Psychology, University College London, United Kingdom*
[7]*Medical Research Council Cognition and Brain Sciences Unit, University of Cambridge, United Kingdom*